7-1-2010

Dynamic photon painting

Zhe Chen
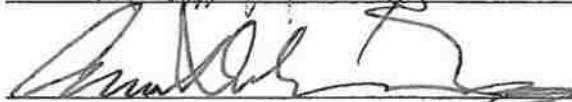
Student Name   Zhe Chen

Zhe Chen

Graduate Unit (Department)   Computer Science

Computer Science

This thesis is approved, and it is acceptable in quality
and form for publication:

Approved by the Thesis Committee:

Shuang Luan, Chair

Adam Hecht

Daliang Cao

Dynamic Photon Painting

BY

Zhe Chen

B.S., Software Engineering, Huazhong University of Science and Technology, 2007

THESIS

Submitted in Partial Fulfillment of the
Requirements for the Degree of
Master of Science

Computer Science

The University of New Mexico
Albuquerque, New Mexico

July, 2010

ACKNOWLEDGMENTS

Dynamic Photon Painting

BY

Zhe Chen

ABSTRACT OF THESIS

Submitted in Partial Fulfillment of the
Requirements for the Degree of

Master of Science

Computer Science

The University of New Mexico
Albuquerque, New Mexico

July, 2010

Dynamic Photon Painting

by

Zhe Chen

B.S., Software Engineering, Huazhong University of Science and Technology, 2007

M.S., Computer Science, University of New Mexico, 2010

ABSTRACT

Photon-based radiosurgery is widely used for treating local and regional tumors. The key to improving the quality of radiosurgery is to increase the dose falloff rate from high dose regions inside the tumor to low dose regions of nearby healthy tissues and structures. Currently, most radiosurgeries rely on focusing a number of external radiation beams to create a sharp dose falloff. As the number of focused beams increases, the contributions from each beam will inevitably decrease, and hence an improved dose falloff will be obtained. However, with most radiosurgeries being delivered in a step-and-shoot manner, the number of external beams is limited to a few hundred. For example, Gamma Knife radiosurgery, which has long been a "gold standard" for radiosurgery, uses about two hundred beams. In this research, we investigated the use of Dynamic Photon Painting (DPP) to further increase dose falloff rate. The key idea of DPP is to treat a target by moving a beam source along a dynamic trajectory, where the speed, directions and even dose rate of the beam source change constantly during irradiation. A number of studies regarding DPP were carried out in this research. We found that DPP can create a dose gradient that rivals proton Bragg Peak and outperforms

Gamma Knife radiosurgery. These promising results indicate that DPP has the potential to significantly improve current photon-based radiosurgery.

TABLE OF CONTENTS

CHAPTER 1 INTRODUCTION

Radiosurgery is one of the most effective ways to treat local and regional tumors, especially for brain tumors. The steep falloff rate of dose distribution is so that critical structures nearby the target will receive a low dose while the center of the tumor will receive a high dose [1][13][26][44]. Thousands of successful treated cases show that radiosurgery is a very safe and efficient method for treating cancers and avoids loss in quality of life compared to other more invasive methods such as surgery or chemotherapy [2][51].

The quality of radiosurgery is determined by the dose falloff rate from high dose regions to low dose regions. Currently, the cross-firing technique is widely used to increase the dose falloff rate. In this technique, a large number of radiation beams focus on a target to create a high dose region around the focusing point [26][34][37]. Intuitively, if the number of beams is increased, the contribution of each beam will inevitably decrease, resulting in a lower dose to the tissues and structures some distance away from the target. Thus, increasing the number of radiation beams should give us sharper dose falloff rate (see Figure 1).

Most current radiosurgeries are delivered in a step-and-shoot approach. This limits the number of beams to a few hundreds due to various practical and physical constraints. For example, in Gamma Knife radiosurgery (see section 2.3 for more details) [2][12][13][14][16][25][26][27][32][34][35][36][37][48][51][53][54][63], the number of

beams is limited to about two hundred. Physically, it is not possible to drill a large number of apertures in a fixed size metal without eventually causing interference among them. For intensity-modulated radiation therapy (IMRT) [20][61], it is usually not practical to deliver more than a dozen beams due to prolonged treatment time. Even with rotational techniques, such as Tomotherapy [29][41], intensity-modulated arc therapy (IMAT) [60], volumetric modulated arc therapy (VMAT) [45], and arc-modulated radiation therapy (AMRT) [58], the maximum number of beams is still limited to a few hundred.
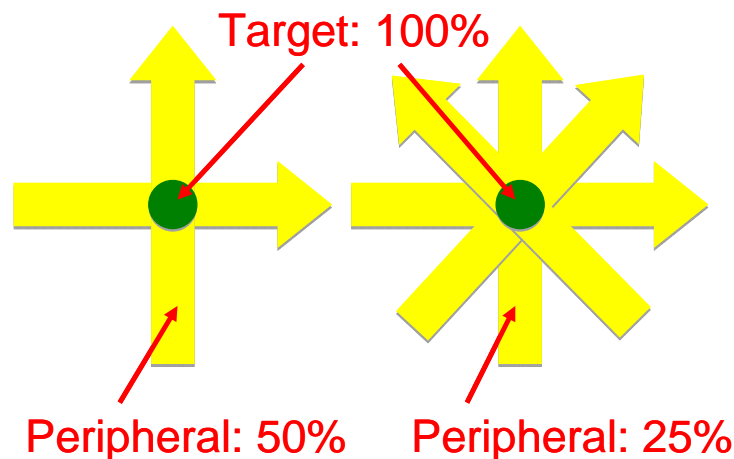
Figure 1 Illustrating the cross-firing technique used in radiosurgery.

We believe in order to further improve the focusing power of radiosurgery, dynamic strategies must be involved, in which a beam source moves around a focused point in a 3D trajectory with constant change of dose rate, speed, and beam directions. The dynamic motion is equivalent to focusing tens of thousands of beams at a common point and will therefore create kernel with a much sharper dose falloff. We call this

approach dynamic photon painting (DPP). The dose distribution from this convergence of tens of thousands of beams on a small volume is used as the DPP kernel.

In this thesis, we studied the potential dosimetric impact of DPP. The rest of the thesis is organized as follows: Section 2 introduces some background knowledge. Section 3 introduces dynamic photon painting and studies the impact of dynamic strategies on dose gradient. Section 4 explores the potential of DDP for treatment planning. We conclude in Section 5 and discuss some of our current ongoing research.

CHAPTER 2 BACKGROUND

2.1 Fundamental Physics

In this thesis, we will focus on photon based radiosurgeries. In this section, we briefly discuss the fundamental physics underlying photon based radiosurgeries.

2.1.1 High Energy Photon Production

Generally speaking, high energy photons used in current radiosurgeries are produced either by radioactive decay from Cobalt-60 sources or bremsstrahlung interactions in the linear accelerator. In the linear accelerator, electrons are accelerated in the electric field to a high energy and then collide with a metal target. The deceleration in the target releases photons in a process called bremsstrahlung. The photons produced from Cobalt-60 decay, coming from the nucleus, are γ-rays whereas the photons produced from electron interactions such as in the linear accelerator bremsstrahlung method are called x-rays.

Typically photons produced by different sources are heterogeneous in energy. For example, the energies of γ-rays emitted by Cobalt-60 are 1.17 and 1.33MeV. The energy spectrum of X-ray from linear accelerator shows a continuous distribution of energies for the bremsstrahlung photons superimposed by characteristic radiation of discrete energies. The energies of photon beams created by 6MV accelerator are continuous from 0 to 6MeV with a maximum yield around 2MeV.

2.1.2 Photon Interaction with Matter

When photons pass through matter, they interact in three ways: photoelectric effect, Compton effect and pair production. For the energy range of radiosurgery photons, the predominant interaction is the Compton effect, where the incident photons collide elastically with electrons. During this elastic collision, kinetic energy is transferred from the incident photon to an electron. These recoil electrons, called secondary electrons, will produce ionization and excitation along their path as they travel through matter. On a cellular level, these ionizations will damage DNA and cause cell death [4][42].

2.1.3 Percent Depth Dose, Tissue Maximum Ratio and Off Center Ratio

Percent depth dose curve relates the absorbed dose deposited by a radiation beam in a medium, such as water for our data. Figure 2 (a) shows the percent depth dose of Cobalt-60 with 80cm SSD. The curve presented starts at 5mm, and so the initial dose build up is not displayed. Another two important concepts of a radiation beam are Tissue Maximum Ratio (TMR) and Off Center Ratio (OCR). TMR is defined as the ratio of the dose at a given point in phantom to the dose at the same point at the reference depth of maximum dose. OCR is the ratio of the absorbed dose at a given off-axis point relative to the dose at the central axis at the same depth. Figure 2 (b) shows the TMR of Cobalt-60 and 6MV accelerator, also starting at 5mm. Figure 2 (c) shows the OCR of 6MV accelerator. (PDD and TMR data of Cobalt-60 are from book "The Physics of Radiation Therapy" [30] at Appendix 14 and 15. Data from 0mm to 5mm are not available.)

(a)

(b)

6
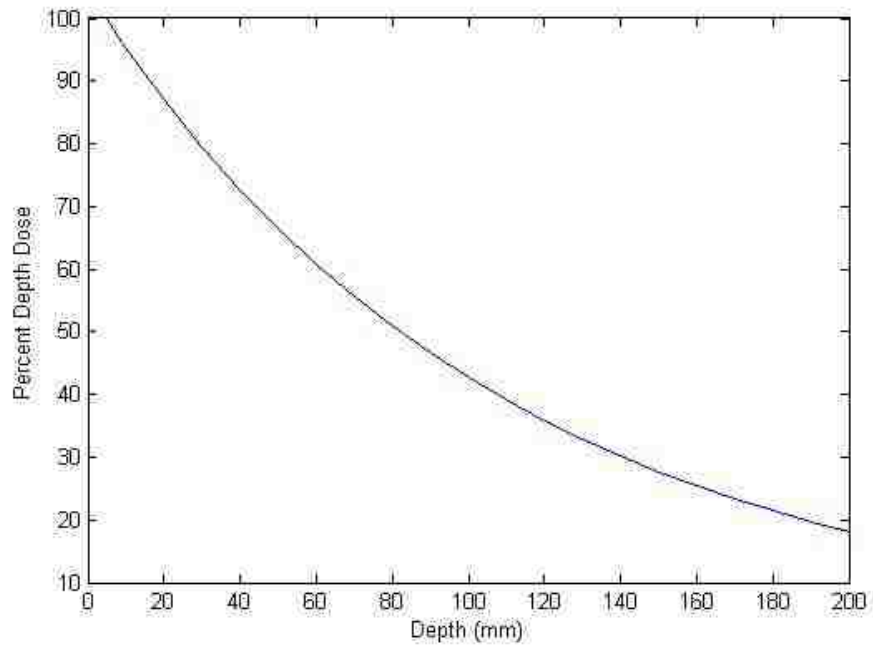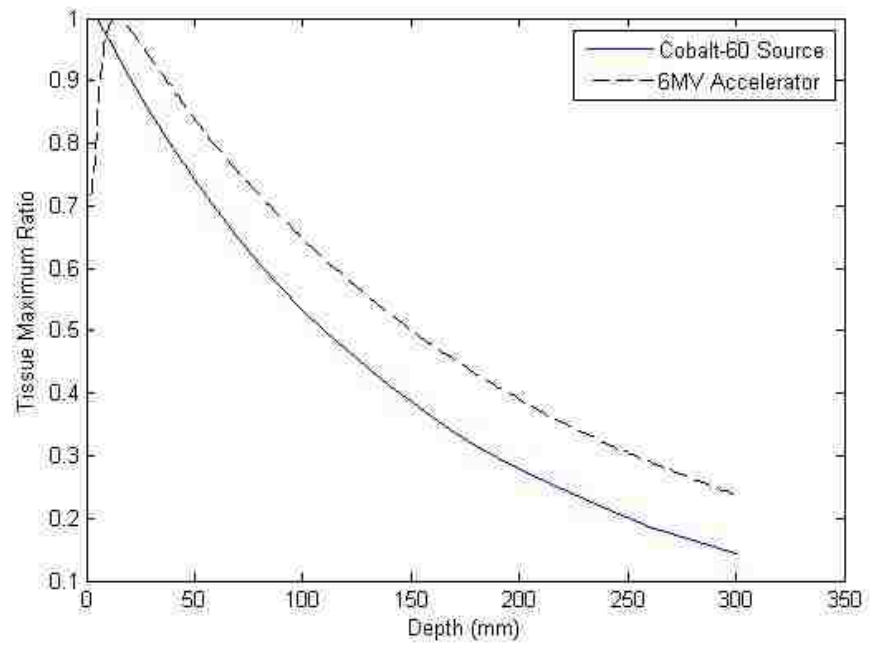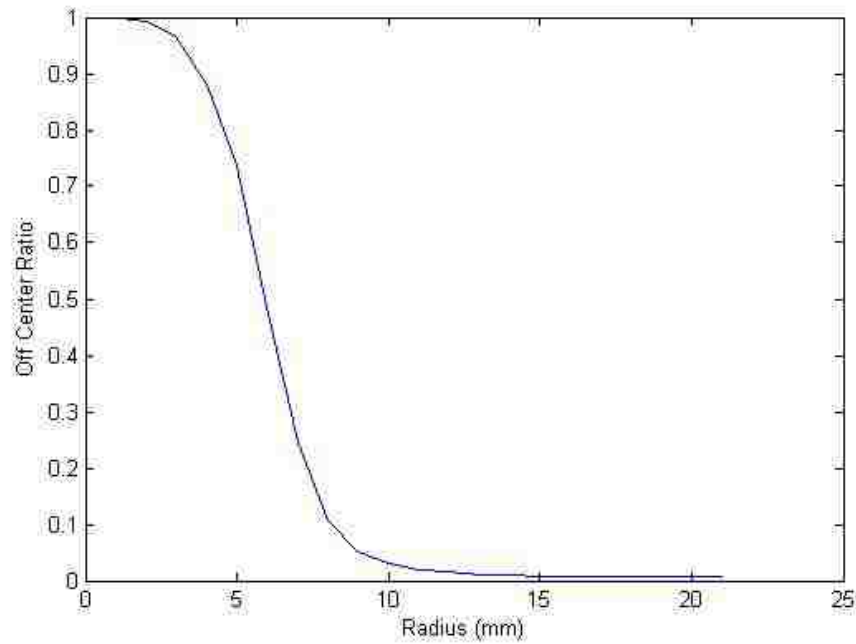
Figure 2 (a) Percent Depth Dose for Co-60, (b) Tissue Maximum Ratio for Co-60 and 6MV accelerator beam, and (c) Off Center Ratio curves for 6MV accelerator beam.

2.2 Radiosurgery

Radiosurgery is a non-invasive medical procedure for various kinds of tumors and functional disorder [1][34][44]. Instead of surgical incision, radiosurgery destroys the tumor by delivering a high dose to it. Since the high energy photons can also damage normal cells along the beam path, the key of a good radiosurgery plan is to maintain a sharp dose falloff from the high dose regions inside the tumor to the low dose regions of nearby healthy structures. The sharper the dose falloff, the better the tumor control and the less the damage to the normal tissues [51].

2.3 Gamma Knife Radiosurgery

Gamma Knife is the most widely used radiosurgery machine. Figure 3 shows a Gamma Knife machine. In Gamma Knife radiosurgery [2][12][13][14][16][25][26] [27][32][34][35][36][37][48][51][53][54][63], γ-rays emitted from radioactive Cobalt-60 sources are used to irradiate tumors. In practical Gamma Knife radiosurgery system, about 200 Cobalt-60 sources are placed in a hemispherical mount and their collimated γ-ray beams are directed onto a single point to create a high dose volume (called "shots" or "kernels"). Current Gamma Knife systems can create high dose volumes of different sizes with external beam collimators and automatic built-in collimators. During Gamma Knife radiosurgery, the patient's head is localized with a stereotactic frame to limit the interference of the patient's motion (see Figure 4). That is also why we call it stereotactic radiosurgery.

Figure 3 The Gamma Knife machine (adapted from Elekta).

Figure 4 The patient is attached to a head frame to prevent movement during treatment (adapted from Elekta).

Current Gamma Knife radiosurgery consists of a planning phase and a delivery phase. In the planning phase, a set of shots of different sizes are used to pack a target volume to create a conformal dose distribution. In this way, the treatment plan becomes delivering a number of shots with determined positions, sizes and beam-on times. In delivery phase, these determined shots are delivered in a step-and-shot manner. The stereotactic head frame provides a reference coordinate system. For each shot, the patient is moved to the coordinate position before receiving the shot.

2.4 CyberKnife Radiosurgery

The CyberKnife radiosurgery system was invented by John R. Adler and Peter and Russell Schonberg of Schonberg Research Corporation [62]. The two main elements of the system are a linear accelerator which produces the radiation beams and a robotic arm which allows the radiation beams to be delivered from any direction as needed (see Figure 5) [15][28][31].

One major advantage of CyberKnife system is its frameless nature, which increases the clinical efficiency. Instead of using a frame to provide a reference coordinate system, CyberKnife uses X-ray image guidance. This avoids anchoring the patient's skull with invasive aluminum or titanium screws and makes it easier to break a long treatment into one to five treatment sessions. However, patient movement needs to be compensated for during the treatment.

2.5 Dynamic Photon Painting

As mentioned previously, the key to radiosurgery is the dose falloff rate. Most current radiosurgeries use a cross-firing technique [34] to improve dose falloff. As the number of beams increases, the dose falloff rate gets better (see Figure 1). However, the number of beams is constrained to several hundred. Thus we propose Dynamic Photon Painting, which moves a beam source around an isocenter in a 3D trajectory (see Figure 6). It is equivalent to focusing thousands of beams on a single point, to increase the dose falloff rate.

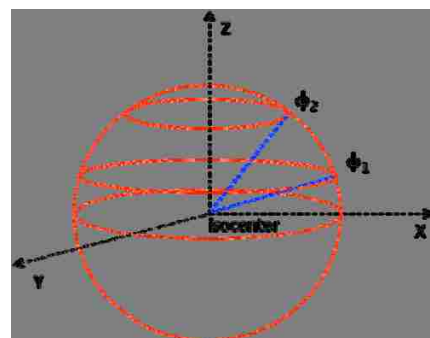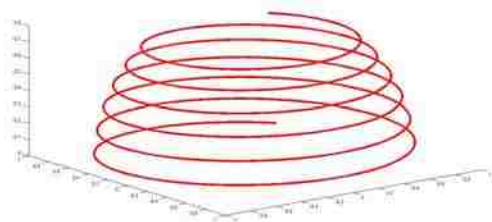Figure 5 The CyberKnife machine (adapted from Accuray)

Figure 6 Illustrate the trajectories of the radiation beam in Dynamic Photon Painting. The beam source rotates around the center of the target from latitude angle ϕ_1 to ϕ_2, and 360° around in longitude angle, about z.

2.6 Least Square Problem

Least square problem, defined as $\min\|Ax-b\|^2$, often occurs as a key sub problem of some larger computational problem, such as radiosurgery treatment planning, intuitively in this model, each column of *A* represents a radiation beam; the column vector *b* represents the ideal dose distribution; the goal of the optimization is to find the optimal "beam on time" for each column (*X*) to create a distribution as close to *b* as possible. Since in reality, "beam on time" must be non-negative, we require $x \geq 0$, which gives the non-negative least square problem (NNLS). In this section, we briefly sketch the solution of least square problem and NNLS problem.

2.6.1 Solving the Least Square Problem

One of the most well known algorithms is from Charles L. Lawson and Richard J. Hanson [33]. The algorithm is based on QR factorization: let A be an $m \times n$ matrix, then there is an $m \times m$ orthogonal matrix Q such that $Q^T R = A$, where *R* is zero below the main diagonal. The key steps of the algorithm is the following: (a) find the QR factorization matrix *Q* of matrix *A*; (b) use matrix *Q* to reduce the original least square problem to $\min\|Rx-Qb\|^2$, where *R* is an upper triangular matrix; (c) solve the least square problem $\min\|Rx-Qb\|^2$.

The following are the key points of solving least square problem. Let *A* be an $m \times n$ matrix with rank k, then $QA = R = \begin{pmatrix} R_{k \times k} & R_{k \times (n-k)} \\ 0_{(m-k) \times k} & 0_{k \times (n-k)} \end{pmatrix}$ where $R_{k \times k}$ is upper

12

triangular with rank k. Observe that $\|Ax - b\|^2 = (Ax - b)^T(Ax - b)$

$= (Ax - b)^T Q^T Q(Ax - b) = (Rx - Qb)^T(Rx - Qb) = \|Rx - Qb\|^2 = (Q(Ax - b))^T(Q(Ax - b))$.

Thus we have an equivalent least square problem $\min\|Rx - Qb\|^2$. Now let

$$y = Qb = \begin{pmatrix} y_k \\ y_{m-k} \end{pmatrix} \ , \quad \text{then} \quad \text{we} \quad \text{have} \quad \|Ax - b\|^2 = \|Rx - Qb\|^2 = \left\| R\begin{pmatrix} x_k \\ x_{n-k} \end{pmatrix} - \begin{pmatrix} y_k \\ y_{m-k} \end{pmatrix} \right\|^2$$

$$= \left\| \begin{matrix} R_{k \times k} x_k + R_{k \times (n-k)} x_{n-k} - y_k \\ - y_{m-k} \end{matrix} \right\|^2 = \left\| R_{k \times k} x_k + R_{k \times (n-k)} x_{n-k} - y_k \right\|^2 + \left\| y_{m-k} \right\|^2 \ . \quad \text{Observe} \quad \text{that}$$

when $R_{k \times k} x_k + R_{k \times (n-k)} x_{n-k} = y_k$, $\|Ax - b\|^2$ reaches the global minimum $\left\| y_{m-k} \right\|^2$.

Notice that there are many solutions, we can pick a straightforward one $R_{k \times k} x_k = y_k$ and

$x_{n-k} = 0$. Since $R_{k \times k}$ is an upper triangular matrix with rank k. It is easy to solve the

equation $R_{k \times k} x_k = y_k$.

To obtain QR factorization [9][17][23], we need to talk about Householder

transformation [7][55] first. Given an m-vector v, which is not the zero vector, there

exists an orthogonal matrix Q such that $Qv = -\delta \| v \| e_1$ with $e_1 = [1 \quad 0 \quad ... \quad 0]^T$ and

$\delta = \begin{cases} +1 & if \ v_I \geq 0 \\ -1 & if \ v_I < 0 \end{cases}$, where v_1 is the first component of v and Q is an $m \times m$

orthogonal matrix. It can prove it easily by define $u = v + \delta\|v\|e_1$ and $Q = I_m - \dfrac{2uu^T}{u^T u}$.

Observe that we just need to apply Householder transformation column by column to

obtain QR factorization.

2.6.2 Solving the Non-Negative Least Square Problem

The NNLS problem is solved by iterative refinement and the answer is approximated by solving a least square problem in every iteration [10][19][21][43][46]. Let $f(x) = (Ax - b)^T (Ax - b)$ and x^* be the optimal solution. Consider two entries $x_i^* > 0$ and $x_j^* = 0$. According to the Kuhn-Tucker Condition [39][50], we must have $\frac{\partial f(x^*)}{\partial x_i} = 0$ and $\frac{\partial f(x^*)}{\partial x_j} \geq 0$. Thus we maintain two sets p and z, p is the collection of the variables in x^* that are positive and z is the collection of variables that are zero. Observe that if we know the correct set p, we can obtain the solution of the NNLS problem by solving the least square problem $\min \left\| A_p y_p - f \right\|^2$, which consists of all the columns indexed by p and then fill in the remaining entries with zeros.

The NNLS algorithm uses the following steps [10][19][21][43][46]:

(1) All variables are in z and the initial solution is $x^{(0)} = 0$.

(2) Let $x^{(k)}$ be the current solution in the current iteration. We split $x^{(k)} = (x_p^{(k)} \quad 0)$. The gradient of $f(x) = (Ax - b)^T (Ax - b)$ is $\nabla f(x) = A^T (Ax - b)$. Observe that $\frac{\partial f(x^{(k)})}{\partial x_i} = 0$ for all $i \in p$. Now if $\frac{\partial f(x^{(k)})}{\partial x_i} \geq 0$ for all $j \in z$, then the optimal condition is met, and we have the optimal solution. If not, then for some $i \in z$, $\frac{\partial f(x^{(k)})}{\partial x_i} < 0$. This implies that we can increase $x_i^{(k)}$ to improve $f(x)$. We add the variable with the most negative $\frac{\partial f(x^{(k)})}{\partial x_i}$ to p.

14

(3) We verify if all the variables in p are strictly positive. This is done using a greedy strategy by solving a least square problem $\min\|A_p y_p - f\|^2$, which consists of all the columns indexed by p. If z_p is feasible, which means $z_p \geq 0$, then $x^{(k+1)} = (y_p^{(k)} \quad 0)$. This implies that our current p is probably too small. We go to step (2) and continue to move variables from z to p. If z_p is not feasible, this means our current p contains variables that should not be in p. We try to move $x_p^{(k)}$ toward z_p as much as possible as long as it is still feasible. The new solution is $x^{(k+1)} = (x_p^{(k)} \quad 0)$. Since some variables may be smaller than zero in $x_p^{(k+1)}$, we need to move them from p back to z. We then solve the least square problem with the updated p.

2.6.3   Running Time Analysis

To solve the least square problem, we need to construct a Householder transformation matrix for each column, which takes $O(n^2)$ time, and then apply this transformation to the entire matrix, which takes $O(n^3)$ time. Since there are n columns, the entire QR factorization cost $O(n^4)$ time. Finally, we need to solve $Rx = g$, where R is a upper triangular matrix. It cost $O(n^2)$ time. Thus the total running time of solving the least square problem will be $O(n^4)$.

However, we can improve the running time. Observe that the Householder transformation can be viewed as multiplying a matrix to a vector c_j.

$$\left(I_m - \frac{2uu^T}{u^Tu} \right)c_j = c_j - \frac{2uu^Tc_j}{u^Tu} = c_j - \frac{2u^Tc_j}{u^Tu}u$$

In this way, apply the Householder transformation to a column can be done in $O(n)$. Then apply the Householder transformation to a $m \times n$ matrix cost $O(n^2)$. Since we need to apply n transformations, the total running time of QR factorization is $O(n^3)$. Then, we can solve the least square problem in $O(n^3)$.

The NNLS algorithm will converge in *3n* iterations, thus the total running time of NNLS algorithm is $O(n^4)$.

2.6.4 Implementation

Using the standard C programming language, we have implemented various versions of the NNLS algorithm, such as the double version, the float version, the float version using Intel Streaming SIMD Extensions (SSE) and parallel computing (multi-thread) [47][56]. Intel SSE instructions take the advantage of the increase of current computers from 32-bit systems to 64-bit systems. These instructions allow us to add four pairs of floating point numbers at the same time. Multi-thread programs take the advantage of current multi-core computers, which split the whole program into several parts and run parallel threads on each CPU core to cut down the running time of programs.

2.6.5 Results

We ran different versions of NNLS program with the same input matrix A (100,000 by 10,000 matrix) and b (100,000 by 1 vector). The following is the running time (in seconds).

Table 1 Running time of various versions of NNLS programs

Program / Optimization flag	Double version	Float version	Multi-thread (8 threads)	SSE	Multi-thread and SSE
No optimization flag	12162.58	11973.46	6096.30	7326.68	5879.14
With flag –O3	4348.40	2640.02	1502.36	2033.73	1496.06

In Table 1, the float version is not significantly faster than the double version when the executable is compiled with no optimization flag; however the running time of float version is only about 60% of that of double version when running with –O3 optimization flag [65]. The running time of the multi-thread version is about 50% of the float version, which is because we can only optimize part of the program. SSE reduced the running time, but not significantly when combined with the multi-thread version. To obtain a better understanding, we compared the running time of the optimized part only.

Table 2 Running time of optimized part

Program / Optimization flag	Float version	Multi-thread (8 threads)
No optimization flag	6764.58	898.76
With flag –O3	1738.83	602.04

Table 2 shows that the running time of multi-thread version was reduced to 13%

of the running time of the original float version, which is more than seven times faster than the original float version. The –O3 optimization flag also cut down the running time of original float version, to 25%.

CHAPTER 3 DYNAMIC PHOTON PAINTING KERNELS

To understand the power and limitation of DPP, we took a CyberKnife cone beam and revolved it in a hemispherical trajectory around a target (see Figure 6). Our CyberKnife beam model is obtained from curve fitting of measured TPR (Tissue Phantom Ratio) and OCR (Off Center Ratio) tables from The University of California San Francisco Radiation Oncology Department (see Figure 7). The functions used for our curve fitting are:

$$\text{TPR}(d) = \begin{cases} \sum_{i=1}^{5} a_i d^{i-1} & \text{for } d < d_{\max} \\ e^{-a_6 \cdot (d - a_7)} & \text{for } d > d_{\max} \end{cases} \qquad \text{and}$$

$$OCR(SAD, r) = 0.5 \cdot \left(erfc\left(a \cdot \left(\frac{r \cdot 800}{SAD} - b \right) \right) + erfc\left(a \cdot \left(\frac{r \cdot 800}{SAD} + b \right) \right) \right), \quad \text{where} \quad d \quad \text{is the}$$

depth and r is the off-center radius of the calculation point, $SAD = SSD + d$ (SAD is the Source Axis Distance and SSD is the Source Surface Distance), and

$$erfc(x) = \frac{2}{\sqrt{\pi}} \int_x^{\infty} e^{-t^2} dt \quad \text{is the error function [66]. For a cone beam with 10mm field size}$$

at $SAD = 800mm$, our curve fitting parameters for TPR are a_1=0.8185, a_2=0.0203, a_3=0.004, a_4=-0.0006, a_5=0.00002, a_6=0.0061, a_7=15, and for OCR a=0.4317 and b=4.9375. (Note that the parameter b here is essentially the radius of the field at 800 mm standard SAD).

The motion trajectory (see Figure 6) of the beam source is described using the following parameters: (1) latitude angular range $[\phi_1, \phi_2]$, (2) longitude angular range $[\theta_1, \theta_2]$, (3) source to axis distances (SAD).
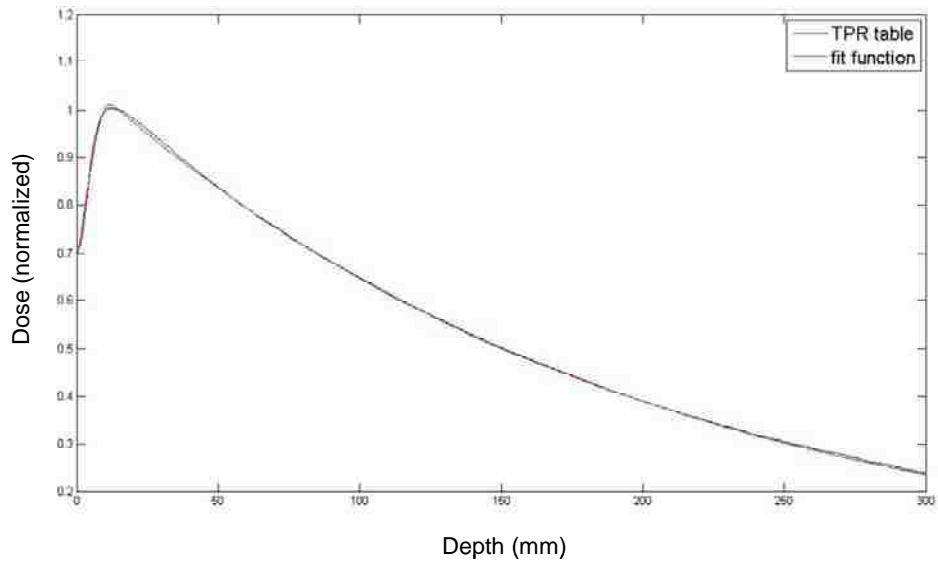

(a)
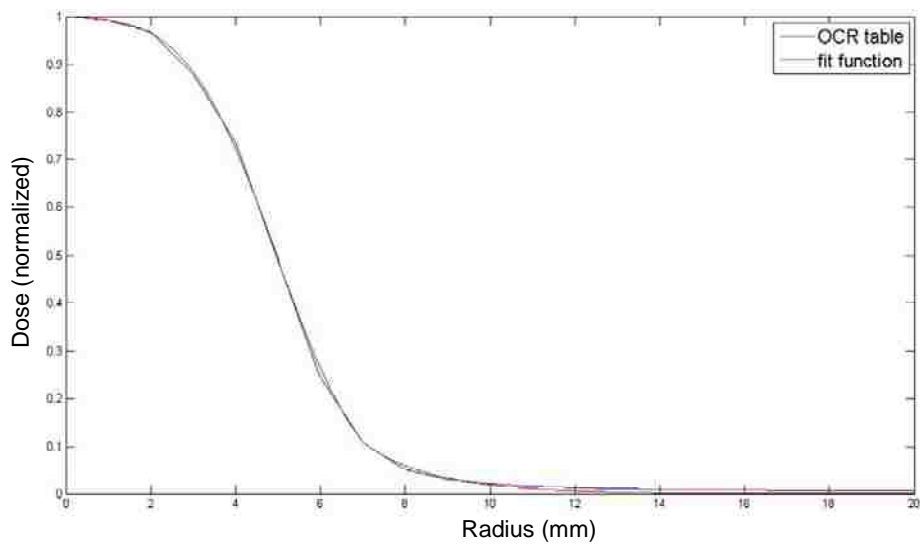
(b)

Figure 7 Curve fitting results for TPR (a) and OCR (b).

By revolving the radiation beam in this dynamic manner, we are able to create the DPP kernels and carry out comparisons with Gamma Knife kernels and proton Bragg Peaks.

3.1 Dynamic Photon Painting vs. Gamma Knife

We compared DPP kernels with Gamma Knife Perfexion 4mm kernels obtained from Elekta [63]. The Gamma Knife kernel is a $41 \times 41 \times 41$ matrix with 0.5mm steps.

Figure 8 shows the dose profile comparison between DPP kernels and Gamma Knife kernels. In this study, the DPP kernels are created using a 10mm cone of the CyberKnife beam model, a SAD of 320mm, and a latitude angular range of 1° to 50°. The SAD is chosen so that the diameter of the DPP kernel at isocenter is also 4mm. (The choice of angular range will be discussed in Section 2.4.) Figure 9 shows the isodose comparisons of the two kernels. In these plots, the planes are defined as in Figure 6. The DPP kernel has a sharper lateral fall off than the Gamma Knife kernel.
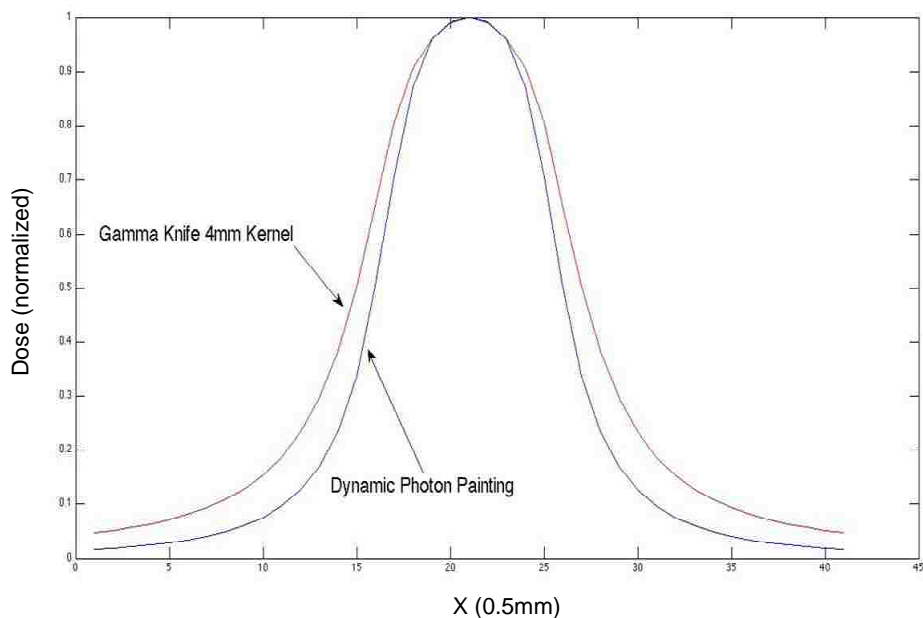
(a)
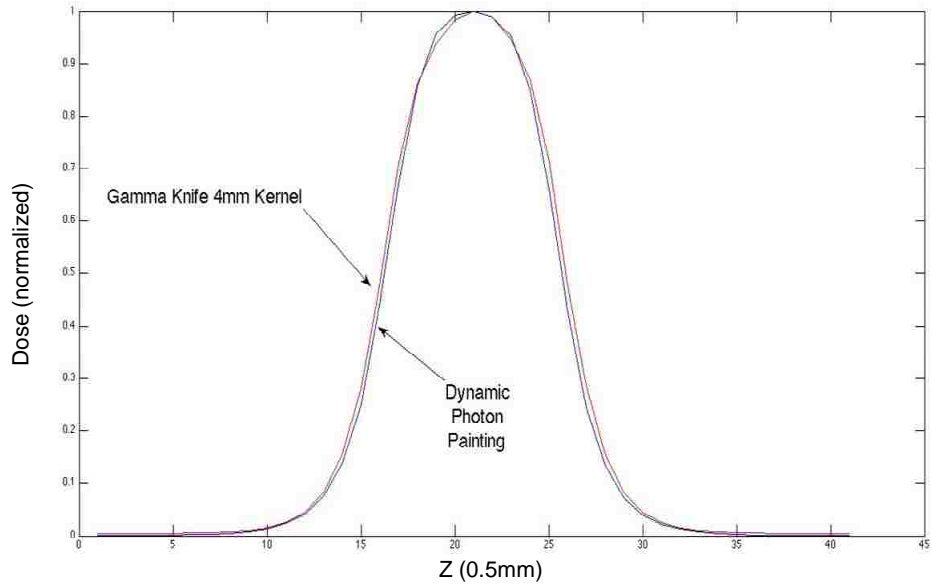
(b)

Figure 8 Dose profile comparisons between DPP kernels and Gamma Knife Perfexion 4mm kernels. (a) Dose profiles in the XY plane. (b) Dose profiles in the XZ plane. See figure 6 for X, Y and Z definitions.


(a)

(b)

(c)
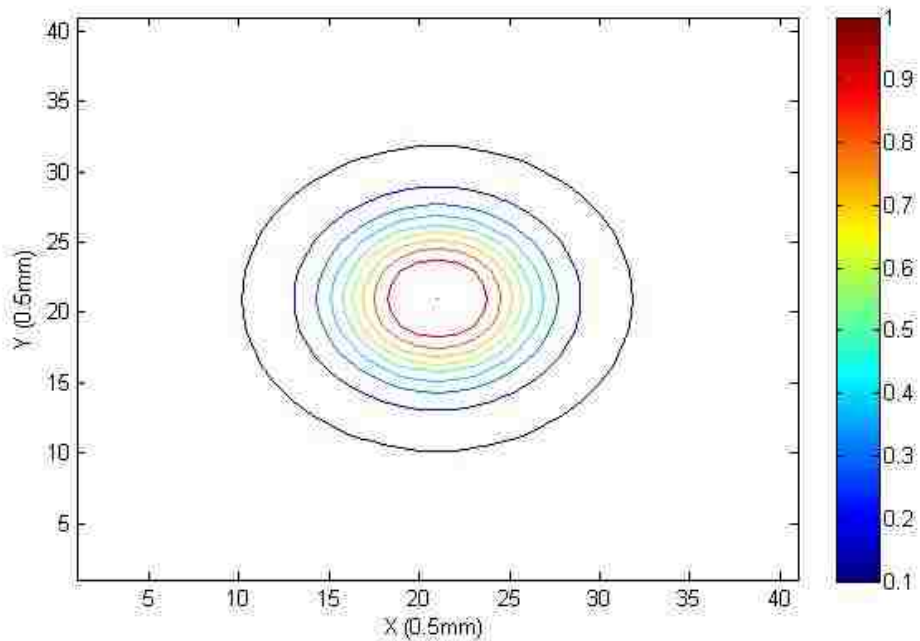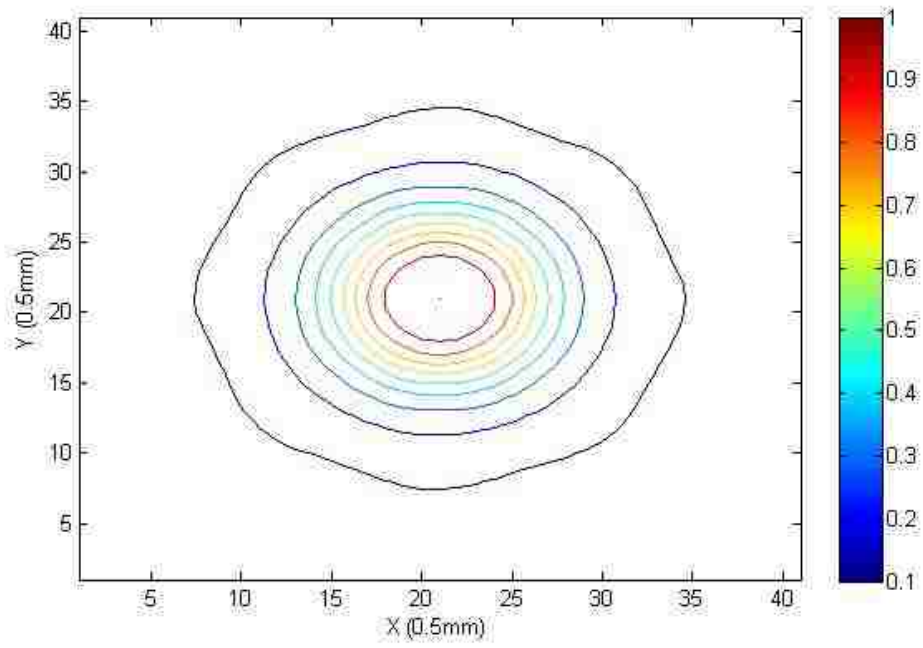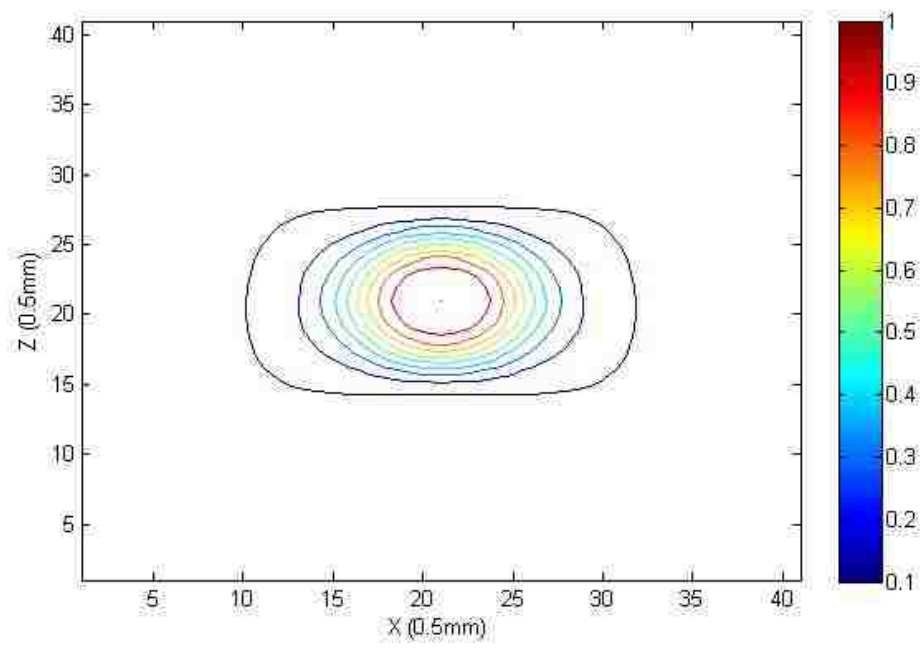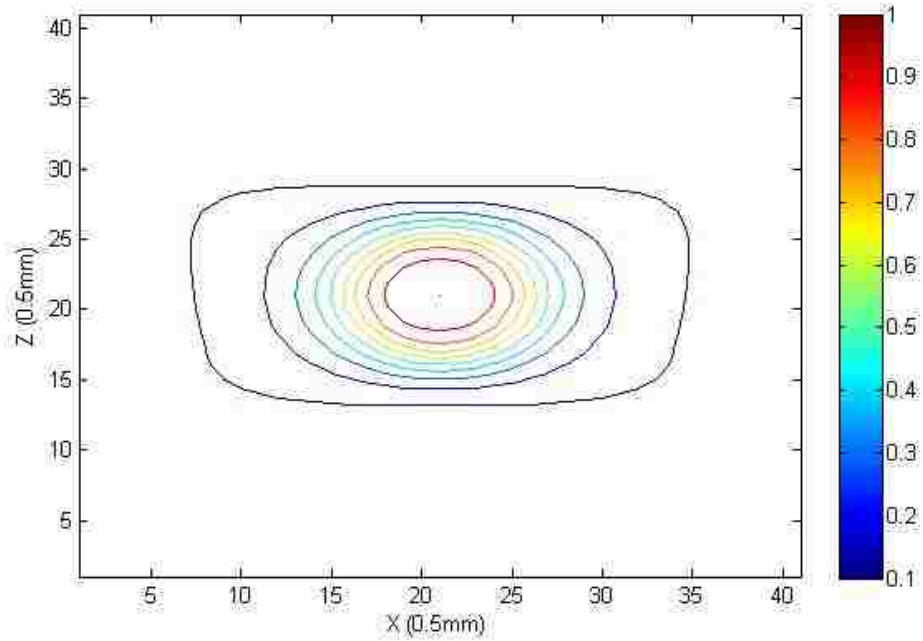
Figure 9 Isodose comparisons between the DPP kernel and Gamma Knife Perfexion 4mm kernels. (a) DPP kernel in the XY plane. (b) Gamma Knife kernel in the XY plane. (c) DPP kernel in the XZ plane. (d) Gamma Knife kernel in the XZ plane. The plot shown contains isodose lines from 10% to 100% with 10% steps.

3.2 Cobalt-60 Source vs. CyberKnife Cone Beam

In order to understand whether our DPP strategy makes the kernel better or the energy of the beam source does, we use the same DPP trajectory but cobalt-60 (Gamma Knife beam source) as the beam source to create kernels to compare with the DPP kernels created with the CyberKnife cone beam. Figure 10 shows the dose profile comparisons between kernels created by the cobalt-60 source and the CyberKnife cone beam. Their

dose profiles are almost identical, which means the impact of the particular beam source is not significant and our DPP strategy makes kernels have better dose falloff.
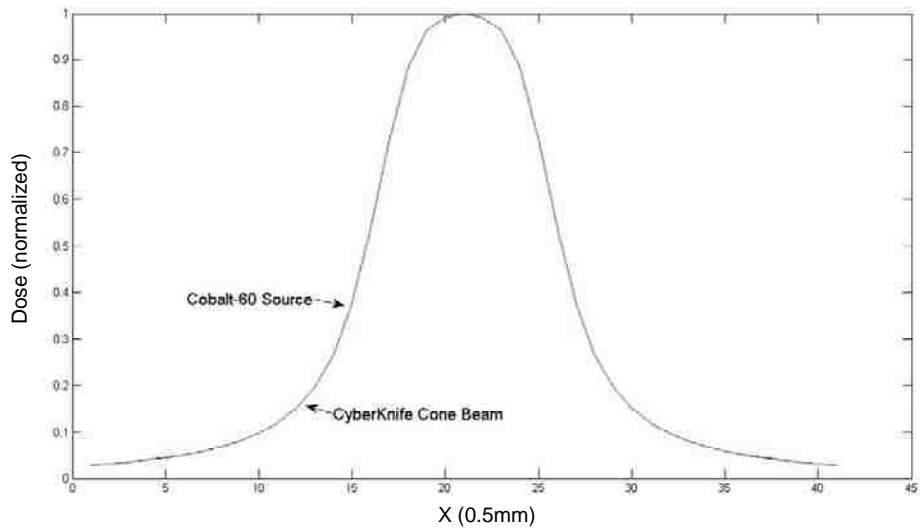

(a)
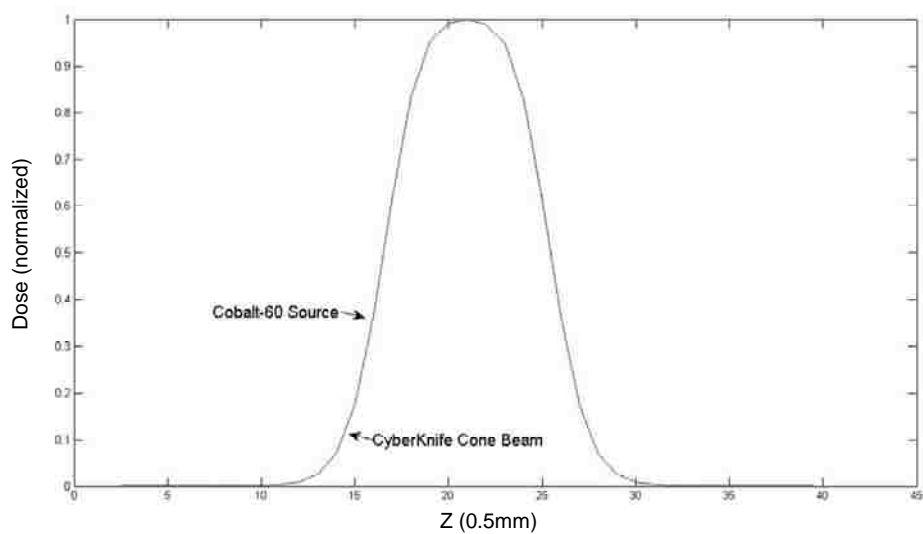
(b)

Figure 10 Dose profile comparisons between kernels created by a cobalt-60 source and the CyberKnife cone beam. (a) Dose profiles in the XY plane. (b) Dose profiles in the XZ plane. See figure 6 for X, Y and Z definitions.

3.3 Dynamic Photon Painting vs. Proton Bragg Peak

We also compared the same DPP kernels with a pristine 116MeV proton beam. The proton was generated in a water phantom with 10^6 primary protons. The beam had a circular Gaussian profile with σ = 2mm. The kernel had a 40mm radius and bins with 0.5mm sides and was calculated using Fluka [64]. Figure 11 (a) shows the dose profile comparison along the distal direction. Figure 11 (b) shows the dose profile comparison in the lateral direction. Figure 11 (c) shows the volume dose histogram comparison. Observe that the DPP kernel deposits most of its energy in a small region.
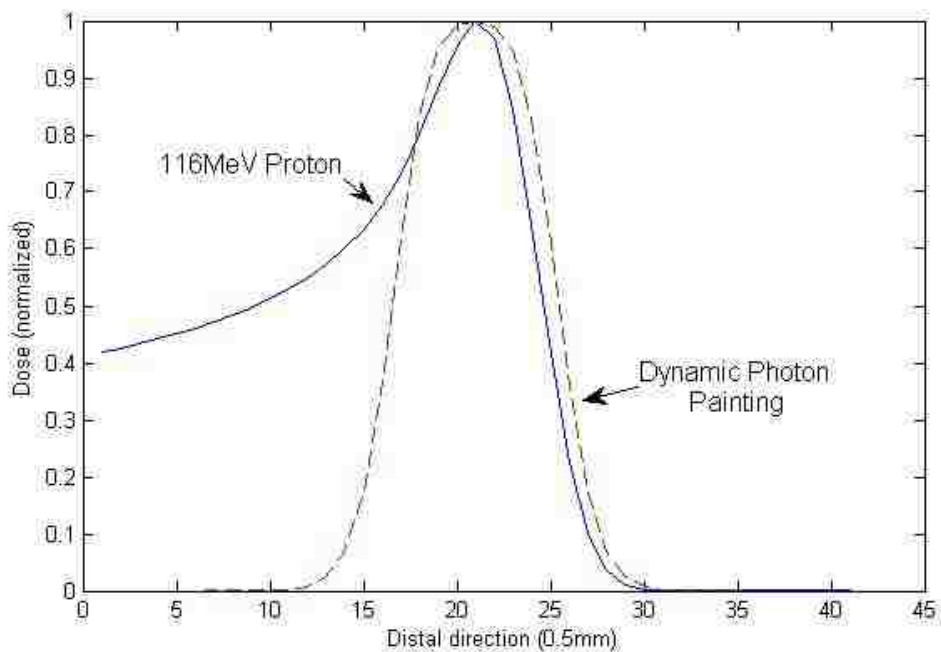

(a)
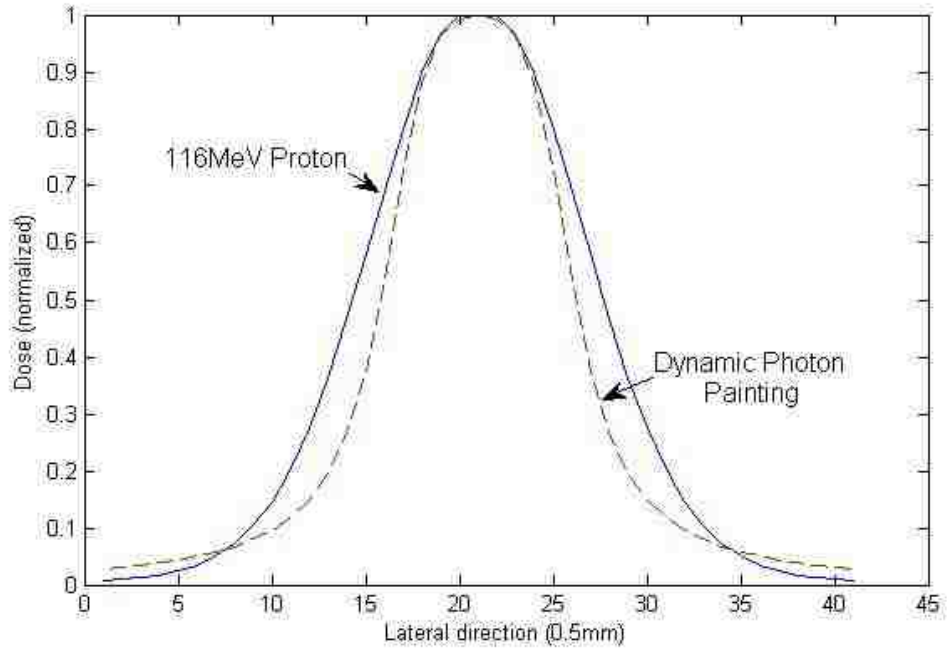
(b)
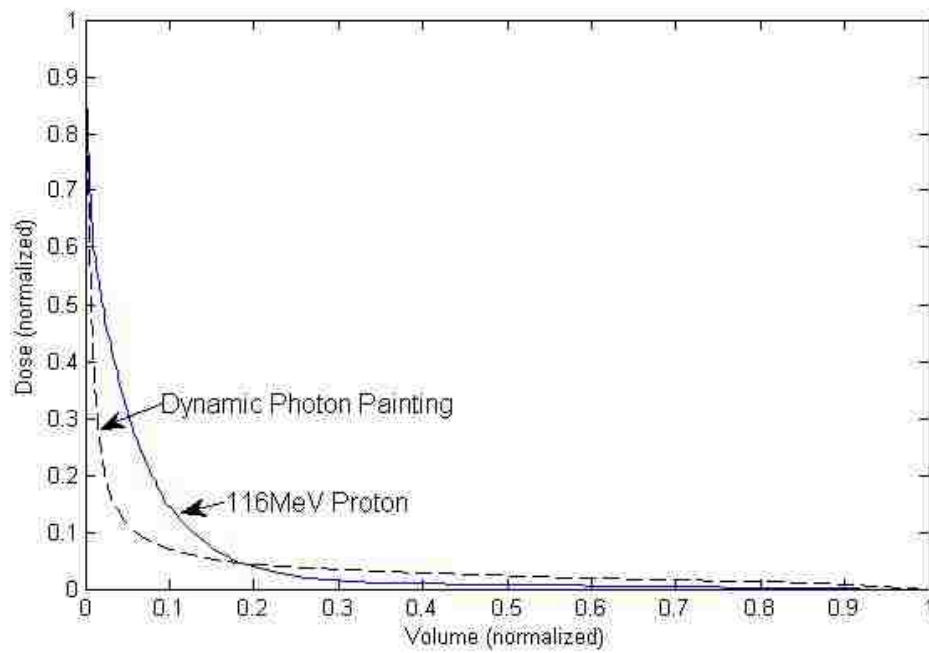
(c)

Figure 11 Comparison between the DPP Kernel and 116 MeV Proton. (a) Profile comparisons in the distal direction. (b) Profile comparisons in the lateral direction. (c) Volume Dose Histograms (VDH) comparisons.

3.4 The Impact of Latitude Angles on Dynamic Photon Painting

We have also studied the impact of latitude angular ranges $[\phi_1, \phi_2]$ on the dose gradient of the DPP kernels. By varying ϕ_1 and ϕ_2, we obtained a set of kernels and compared their dose profiles and isodose distributions.

Figure 12 shows the comparisons of dose profiles with latitude angular ranges 1° to 40°, 1° to 45°, 1° to 50°, 1° to 55°, 1° to 60°, and 1° to 65°. Observe that, as $\Delta\phi = |\phi_1 - \phi_2|$ increases, the dose gradient increases in the XY plane and decreases in the XZ planes. The optimal angular range is a tradeoff between the sharpness of dose in the XY plane to that in the XZ plane. In addition to the above comparisons, we have also studied the impact of ϕ_1, the starting latitude angle when $\Delta\phi$ is fixed. These comparisons are shown in Figure 13. Observe that, as ϕ_1 increases, the isodose distributions in the XZ plane become more and more irregular at low dose levels in comparison to that of the Gamma Knife kernels (Figure 13 (d)).
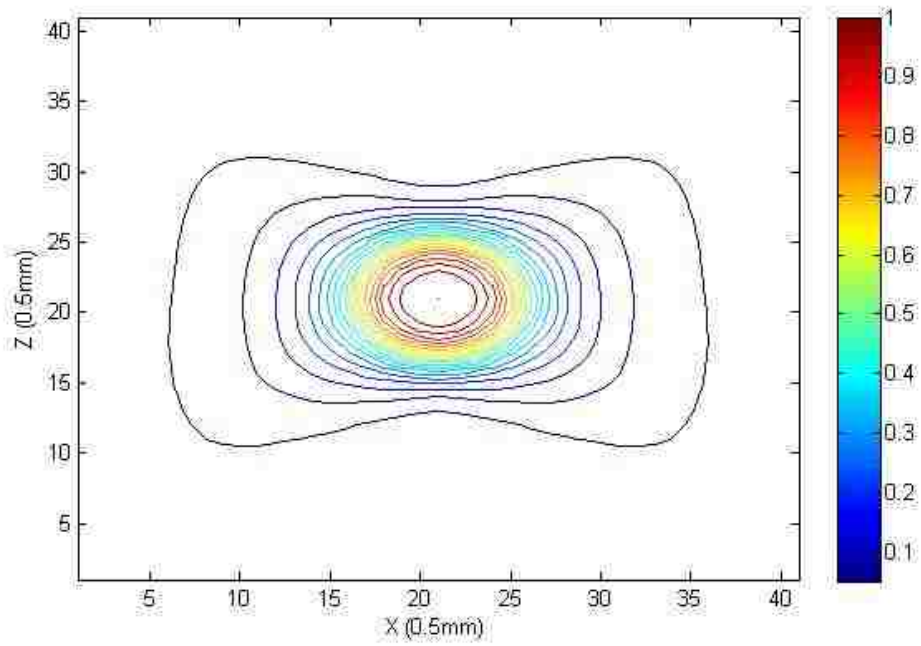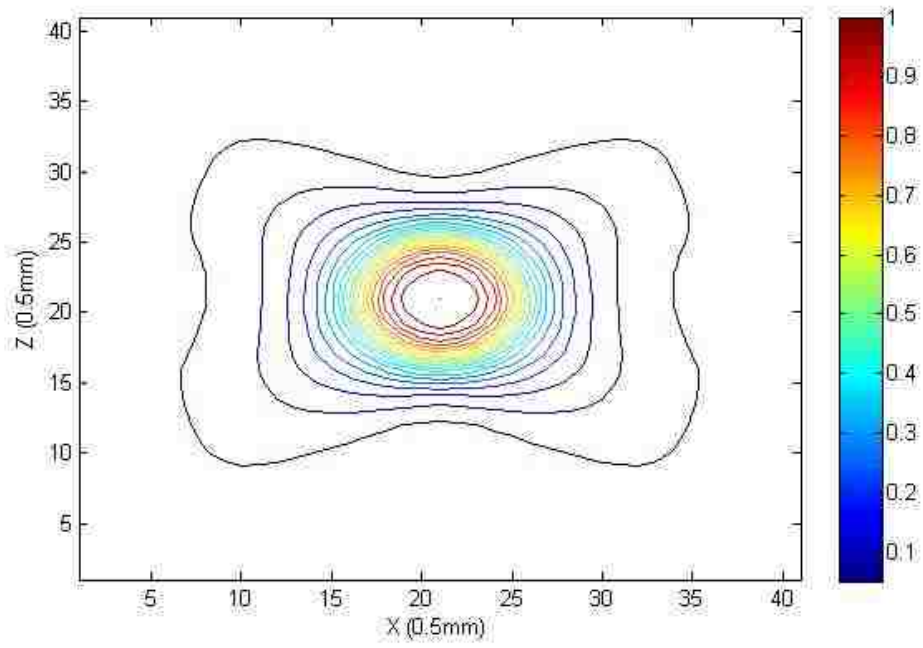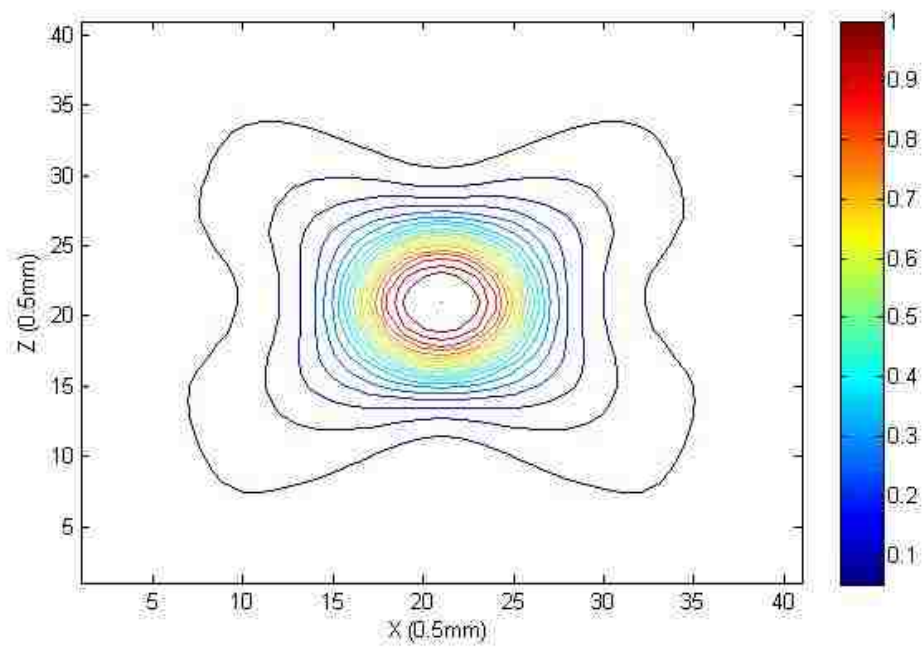

(a)
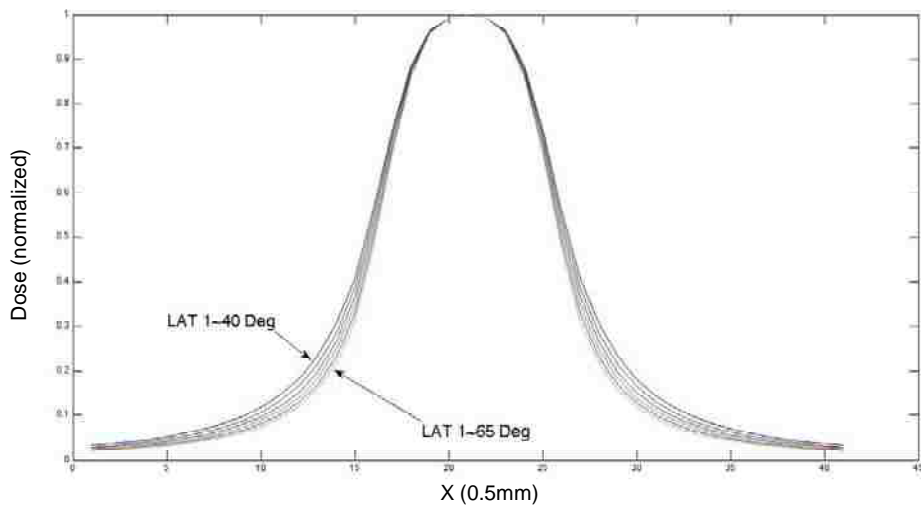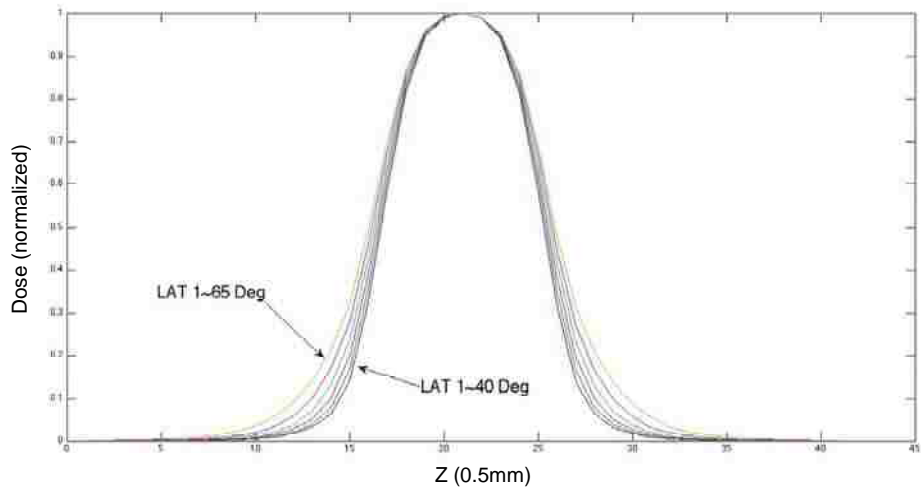
Figure 12 Impact of Lateral Angular range on the dose gradient of DPP kernels. (a) Profile comparisons in the XY plane. (b) Profile comparisons in the XZ plane.
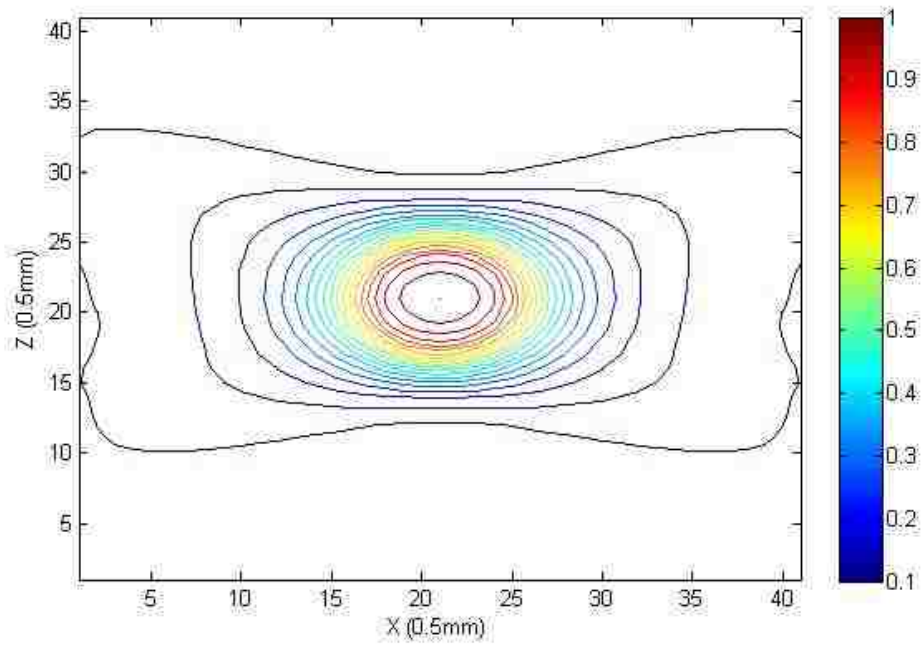
(b)

(c)

(d)

Figure 13 XZ isodose distributions of DPP kernels of different latitude angular ranges. (a) 1° to 50°. (b) 5° to 55°. (c) 10° to 60°. (d) Gamma Knife 4mm kernel. The plot shown contains isodose lines from 5% to 100% with 5% steps.

3.5 The Impact of the ERFC Sharpness Parameter on DPP Kernels

We also studied the impact of the ERFC sharpness parameter on DPP kernels. OCR (Off Center Ratio) curve is fitted using function $f = 0.5*(erfc(a(x-b)) + erfc(a(x+b)))$, where $erfc(x)$ is defined as: $erfc(x) = \frac{2}{\sqrt{\pi}} \int_x^\infty e^{-t^2} dt$ [66]. Mathematically, the parameter a reflects the sharpness, while b represents the width or radius of the field. Figure 14 shows the comparison of dose profiles with $a = 1$ and $a = 10$. Figure 15 shows the isodose comparison of DPP kernels with different ERFC parameters. Observe that the dose falloff rate increases as a increases.
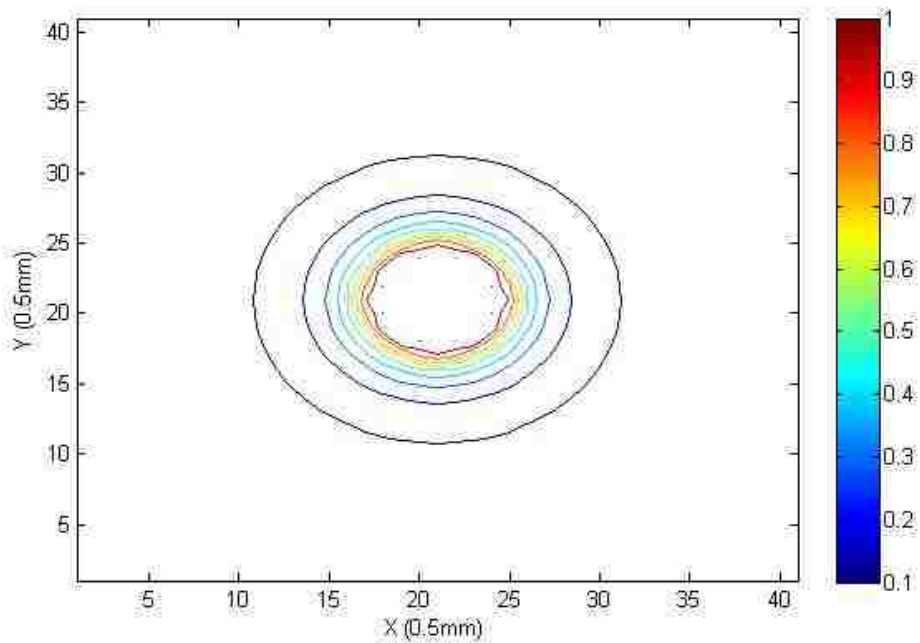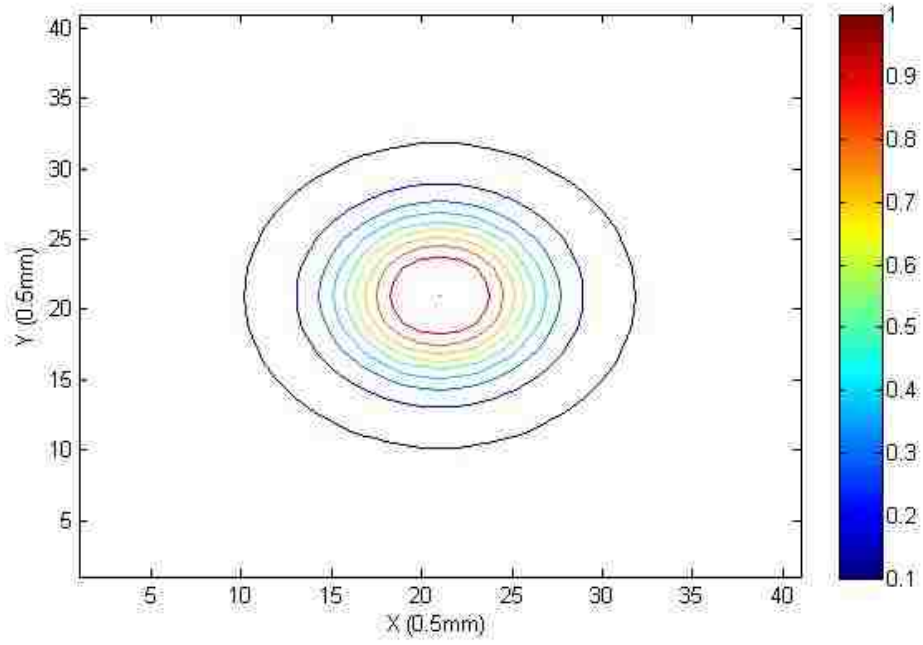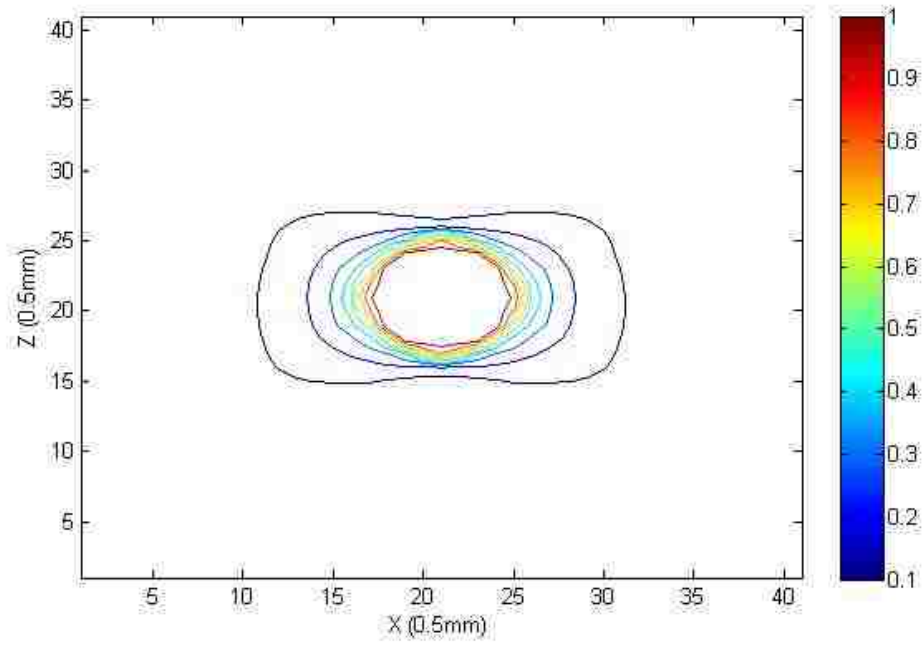

(a)

33
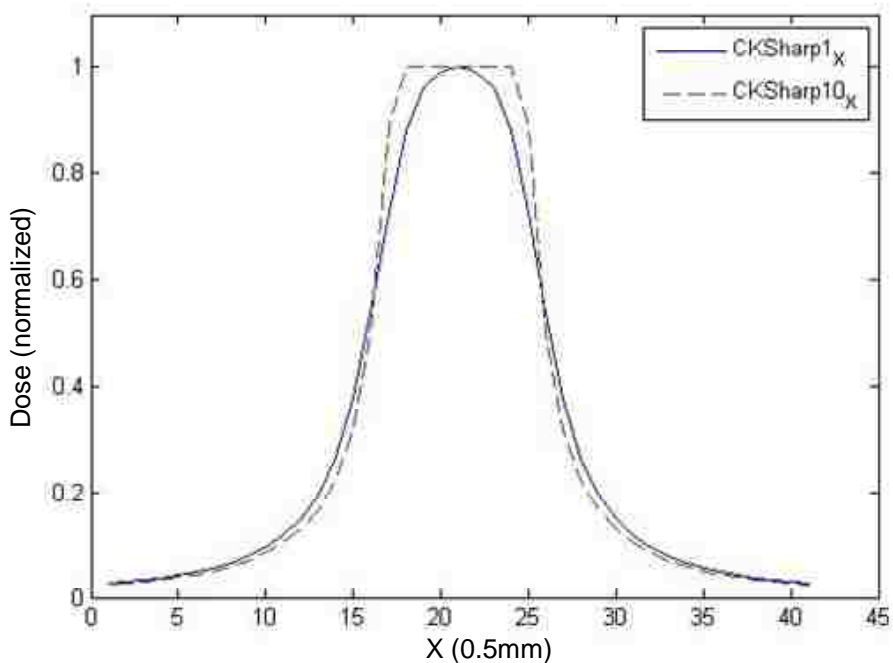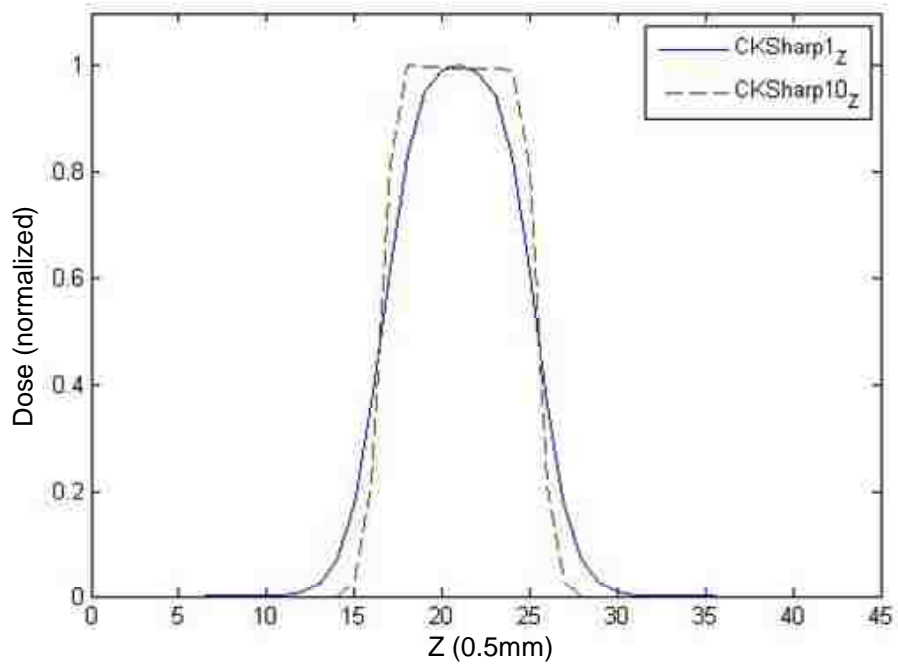
Figure 14 Impact of the ERFC parameter on the dose gradient of DPP kernels. (a) Profile

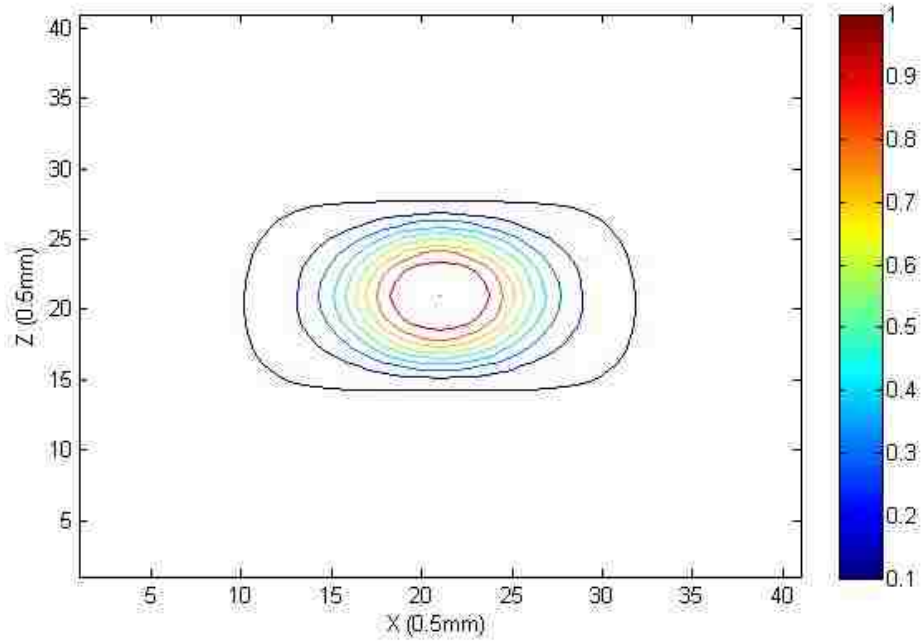comparisons in the XY plane. (b) Profile comparisons in the XZ plane.

(b)

(c)

(d)

Figure 15 Isodose distributions of DPP kernels of different ERFC parameters. (a) Isodose distributions of the DPP kernel with $a = 10$ in the XY plane. (b) Isodose distributions of the DPP kernel with $a = 1$ in the XY plane. (c) Isodose distributions of the DPP kernel with $a = 10$ in the XZ plane. (d) Isodose distributions of the DPP kernel with $a = 1$ in the XZ plane. The plot shown contains isodose lines from 10% to 100% with 10% steps.

CHAPTER 4 Treatment planning results with DPP kernels

One interesting question we have is whether DPP can actually help improve the overall dose distributions in a treatment plan. For comparison purposes, we replaced the Gamma Knife kernels in our Dynamic Gamma Knife Radiosurgery planning system [38] with DPP kernels and compared the dose distributions.

Here we briefly sketch the key idea of dynamic Gamma Knife radiosurgery for the sake of presentation while we refer interested readers to the original paper for more details [38]. Dynamic Gamma Knife radiosurgery is based on the concept of "dose-painting". In our scheme, the spherical high dose volume created by Gamma Knife unit will be viewed as a "paintbrush" and treatment planning becomes painting a 3D tumor volume with a spherical "paintbrush" [37][38]. See Figure 16.
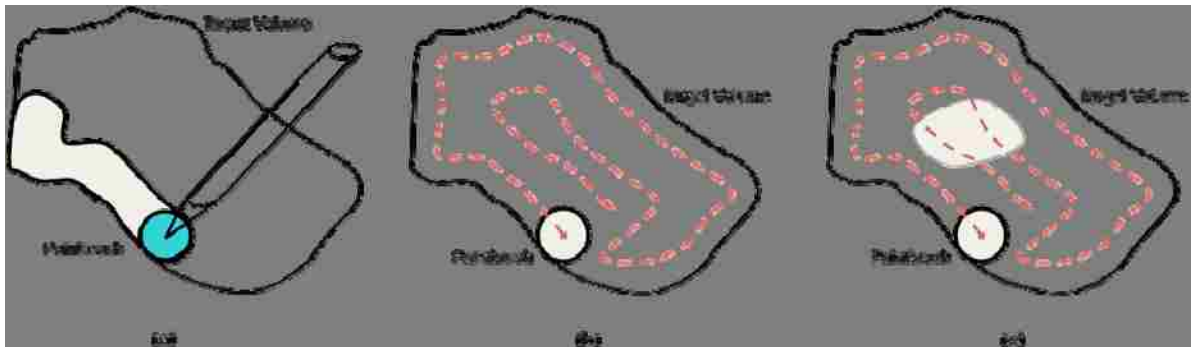

Figure 16 (a) A schematic illustration of the dynamic Gamma Knife radiosurgery concept. (b) Planning dynamic Gamma Knife radiosurgery becomes finding a route for the paintbrush. (c) Sub-region dose escalation can be achieved by slowing down the speed of the paintbrush.

Dynamic Gamma Knife Radiosurgery consists of a planning phase and a delivery phase. In the planning phase, a set of kernels with different size will be used to pack a target volume to create a conformal dose distribution. In this way, the treatment plan becomes delivering a number of kernels with determined positions, sizes and beam-on time. In the delivery phase, those determined kernels will be delivered in a step-and-shot manner.

4.1 Dynamic Gamma Knife vs. DPP using Cyberknife Cone Beams

Two studies were carried out to compare treatment planning result of using DPP kernels and Gamma Knife kernels. In the first study, we used a 3D spherical phantom of 80mm radius with a spherical tumor of 7.5mm radius at the center. Both optimizations were run with identical parameters. To ensure that we got the best Gamma Knife plan possible, only 4mm shots were used in the planning. Figure 17 shows the DVH comparisons. Figure 18 and Figure 19 show the comparisons between dose profiles and isodose distributions. As can be seen from these plots, the DPP plan and the Gamma Knife plan are very similar with the DPP plan slightly better and more uniform.

It is also worthwhile to mention that the precision of these comparisons is limited by the resolution of our Gamma Knife kernels at 5mm. With such a sharp dose gradient, we are approaching the numerical limit. If these comparisons can be done at a much higher resolution, we believe the sharper dose gradient of DPP plans will be more pronounced.
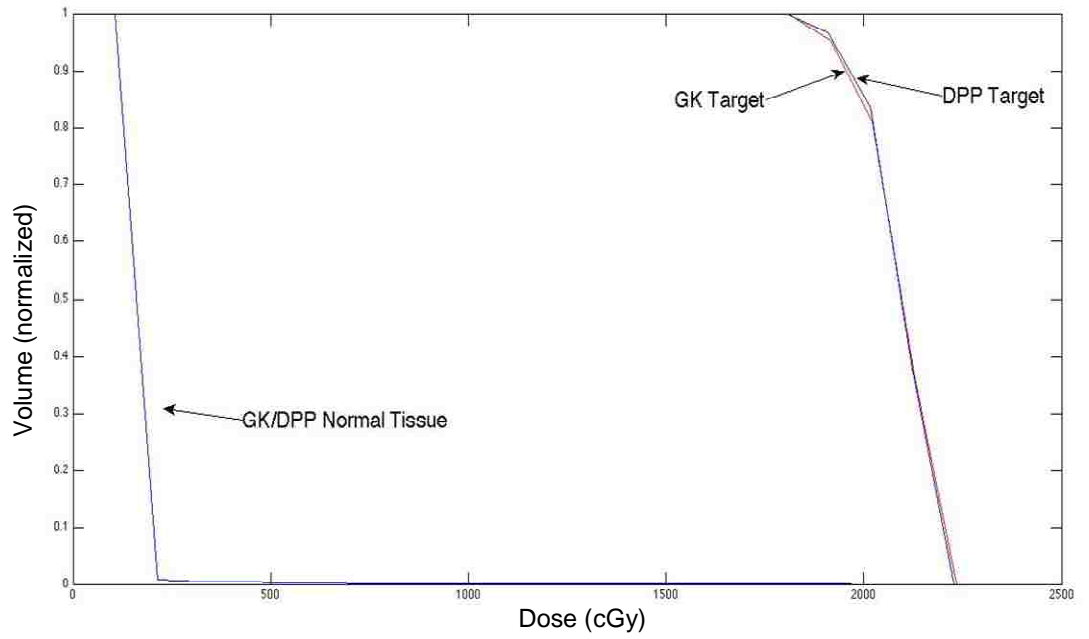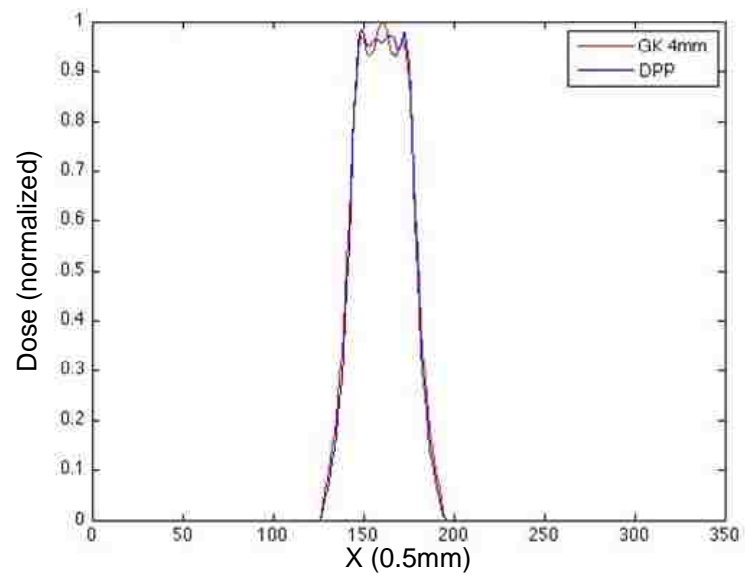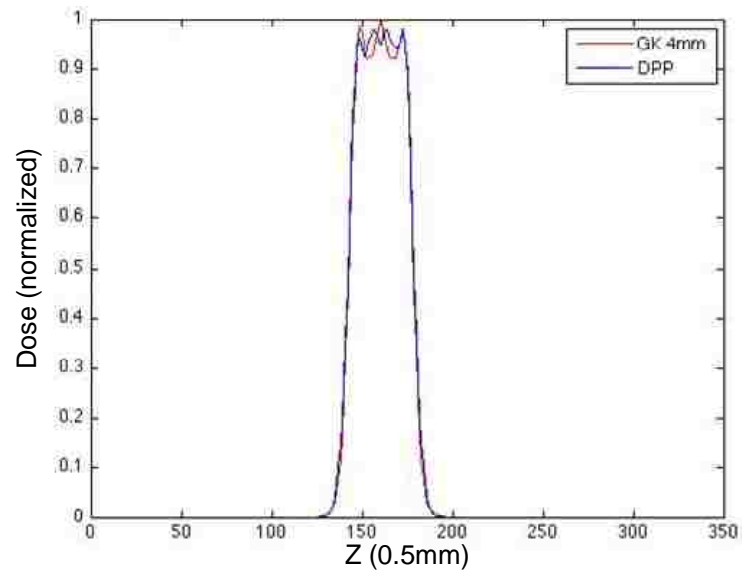
Figure 17 DVH Comparisons of Gamma Knife and DPP using the spherical phantom described in text.
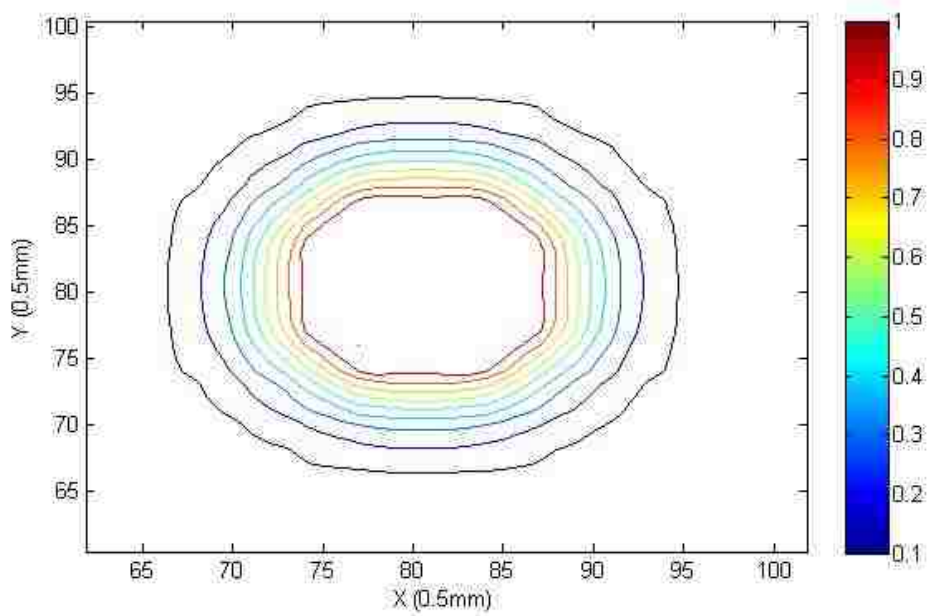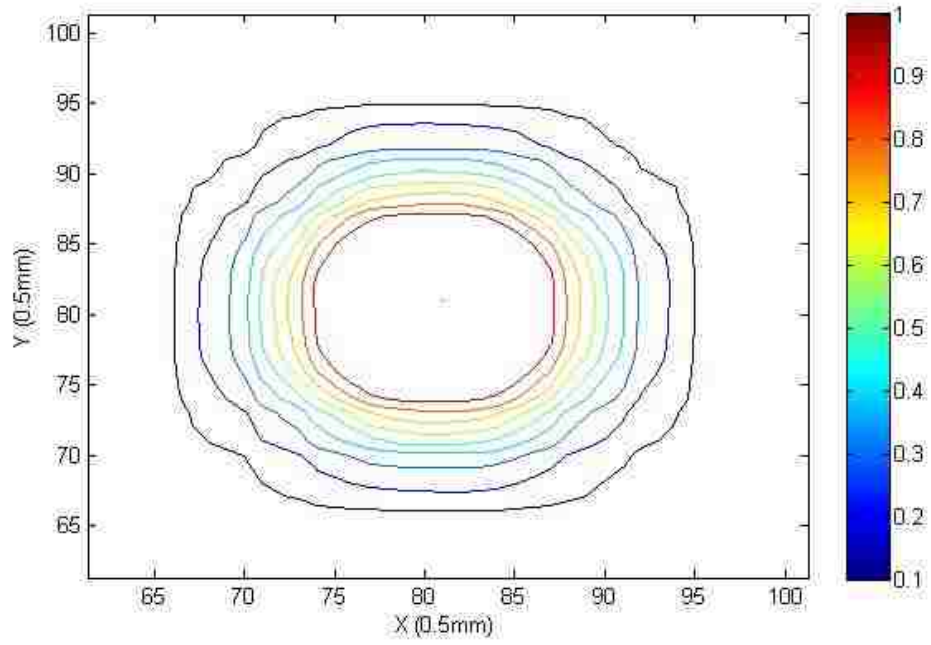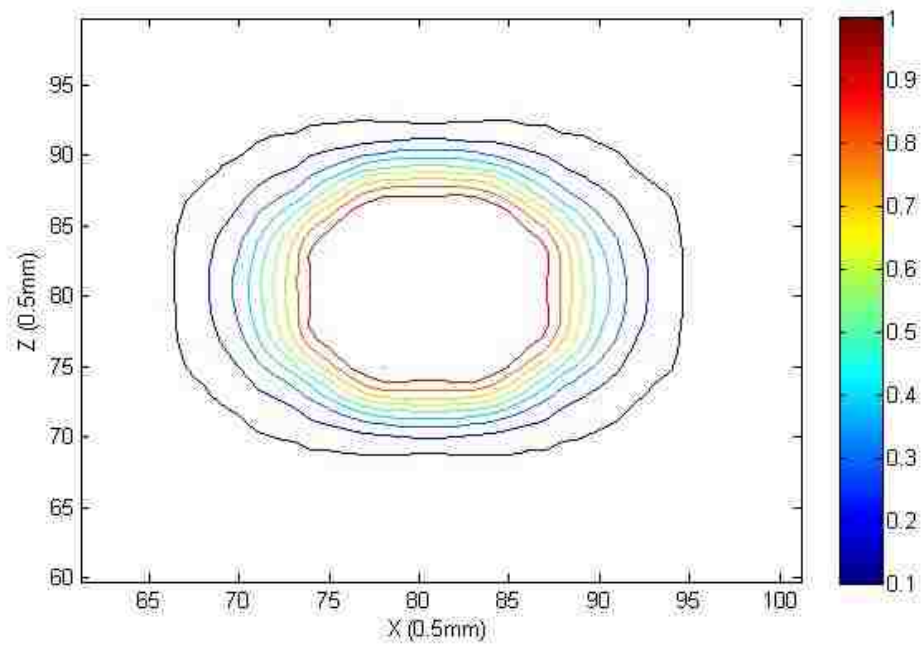

(a)

Figure 18 Dose profile comparisons between a DPP plan (in blue) and a Gamma Knife plan (in red). (a) Dose profiles in the XY plane. (b) Dose profiles in the XZ plane.

(b)

(c)
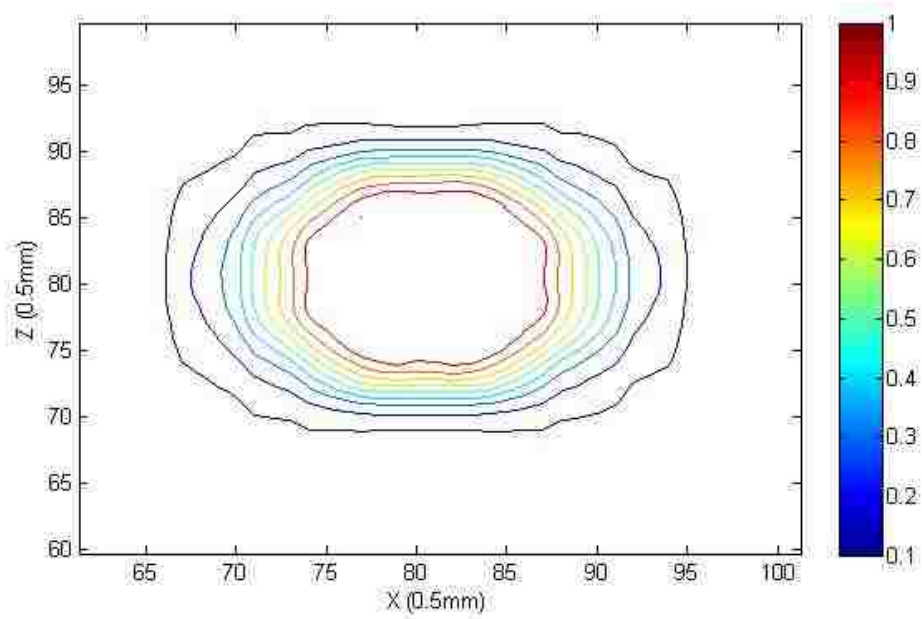
Figure 19 Isodose comparisons between a DPP plan and a Gamma Knife plan. (a) Isodose distributions of the DPP plan in the XY plane. (b) Isodose distributions of the Gamma Knife plan in the XY plane. (c) Isodose distributions of the DPP plan in the XZ plane. (d) Isodose distributions of the Gamma Knife plan in the XZ plane. The plot shown contains isodose lines from 10% to 100% with 10% steps.

We have also used DPP kernels and Gamma Knife kernels for a more challenging phantom, which contains a C-shaped tumor surrounding a spherical critical structure (see Figure 20). The red part is the tumor, surrounding a spherical critical structure.
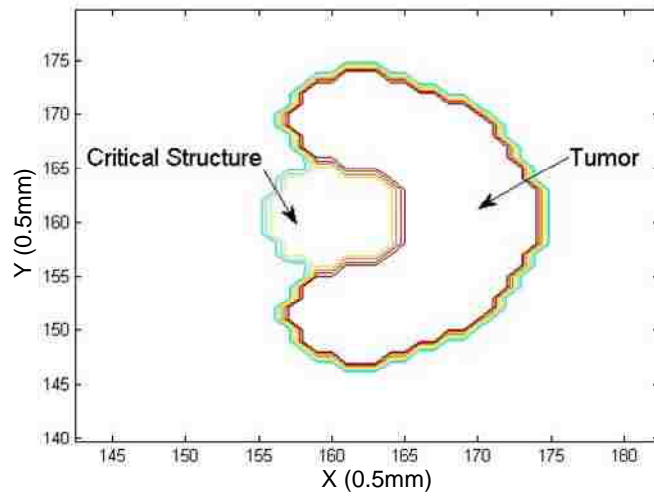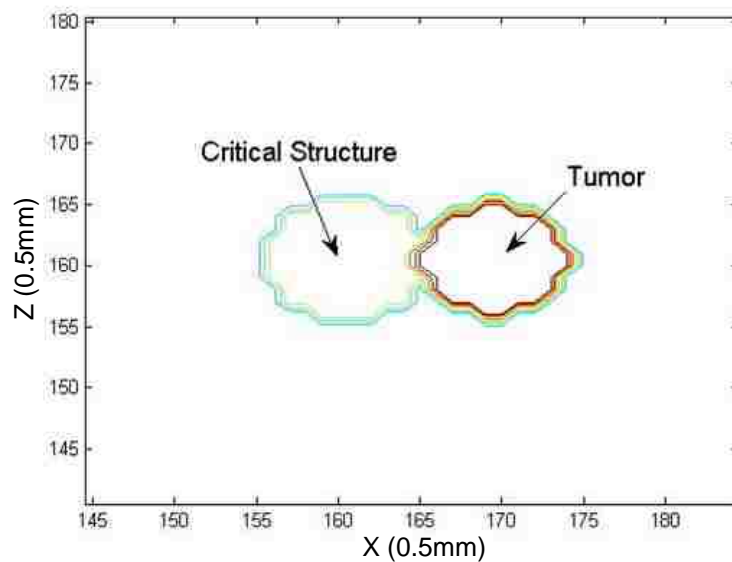
Figure 20 Plot of C-Shaped tumor phantom. (a) Phantom in the XY plan. (b) Phantom in the XZ plan.

Our goal is to let the tumor receive a 2100 cGy dose. Figure 21 shows the DVH comparison. Figure 22 and Figure 23 show the comparisons between dose profiles and between isodose distributions. Observe that the DPP plan is better than the Gamma Knife

plan, since in the DPP plan, the target receives a higher dose and critical structures receive a lower dose than with the Gamma Knife plan. Through the profile comparisons in Figure 22, we notice that the dose at high dose region is similar, while DPP plan has a lower dose at low dose region.
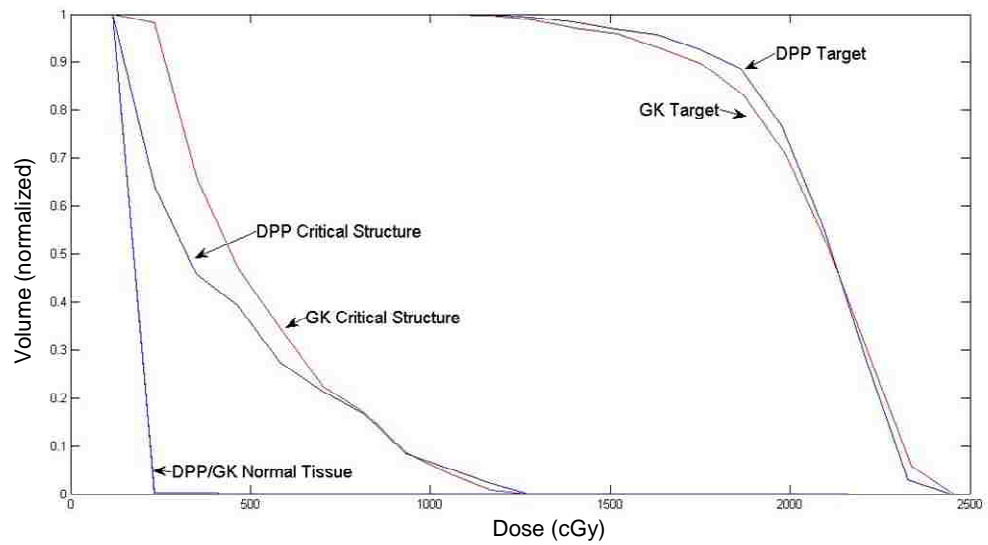
Figure 21 DVH comparison of GK and DPP using the C shaped tumor example
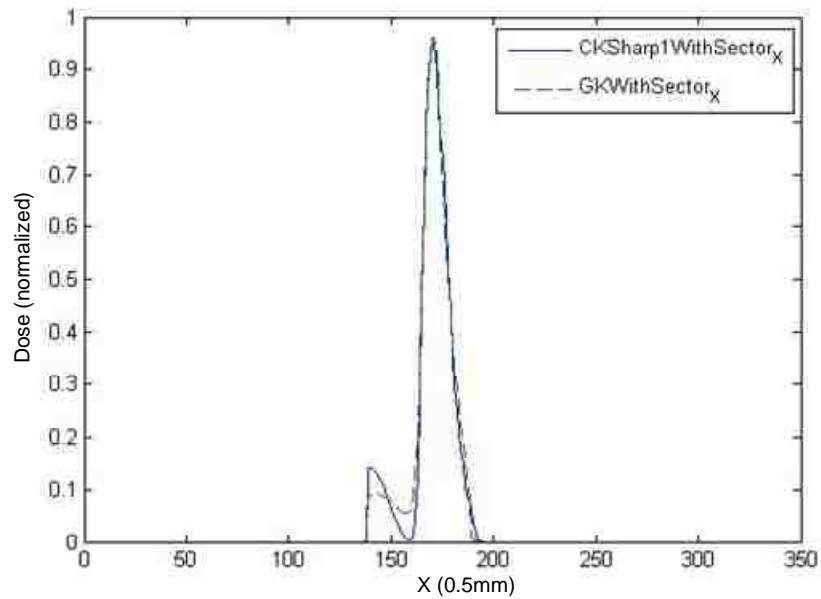
(a)
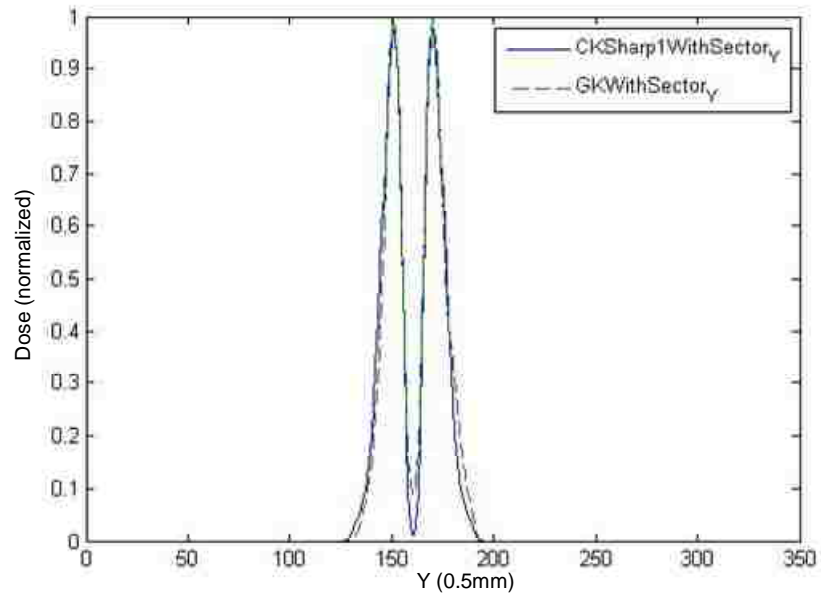
(b)
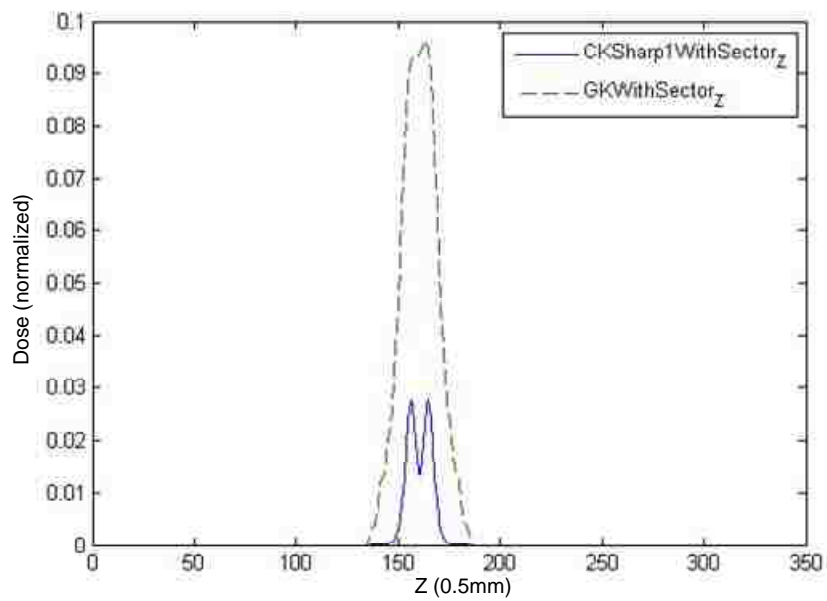
(c)

Figure 22 Dose profile comparisons between a DPP plan (in blue) and a Gamma Knife plan (in green) for the C shaped tumor example. (a) Dose profiles along the X direction. (b) Dose profiles along the Y direction. (c) Dose profiles along the Z direction.

(a)

(b)

46
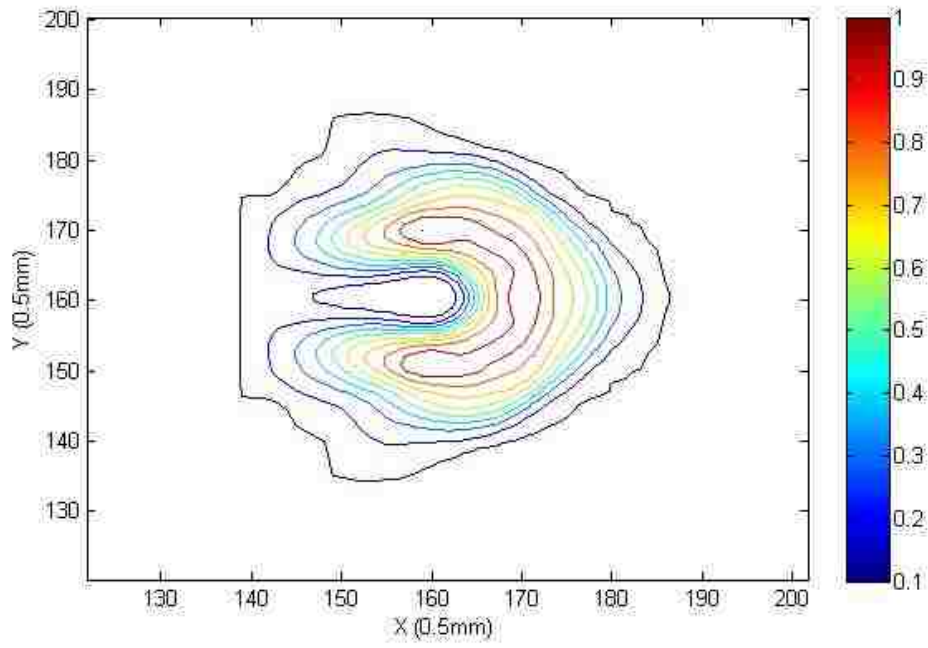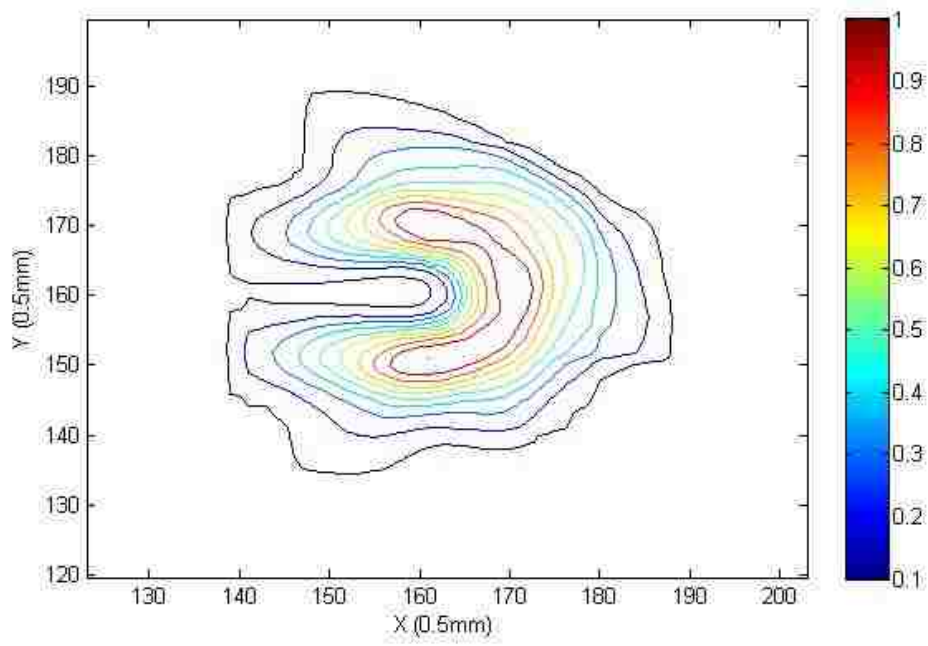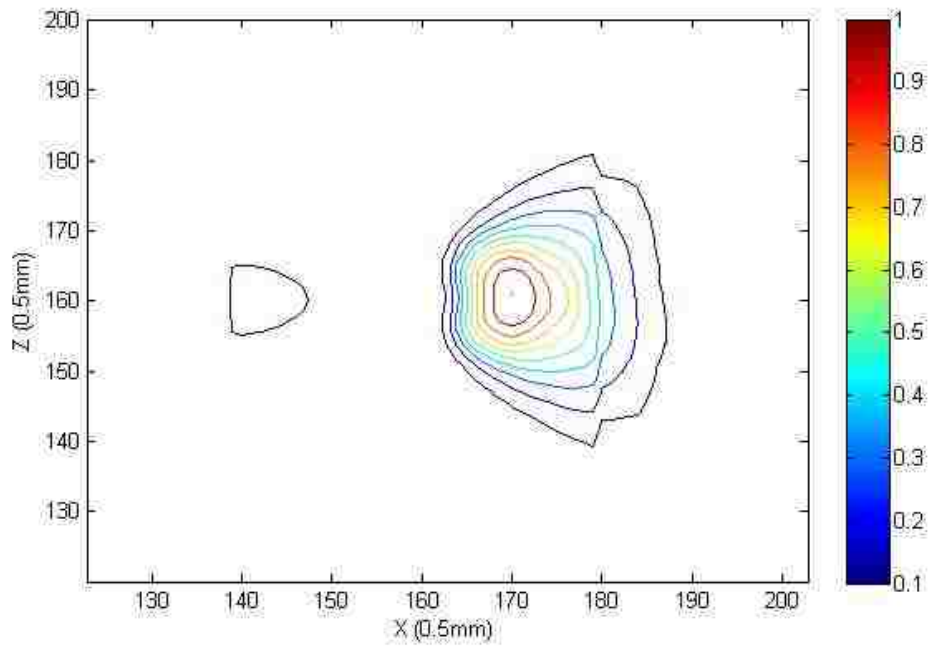
(c)

(d)

Figure 23 Isodose comparisons between a DPP plan and a Gamma Knife plan for the C shaped tumor example. (a) Isodose distributions of the DPP plan in the XY plane. (b) Isodose distributions of the Gamma Knife plan in the XY plane. (c) Isodose distributions

47

of the DPP plan in the XZ plane. (d) Isodose distributions of the Gamma Knife plan in the XZ plane. The plot shown contains isodose lines from 10% to 100% with 10% steps.

4.2 DPP Kernels with Different ERFC Sharpness Parameter

We create two sets of DPP kernels with two different ERFC sharpness parameters $a = 1$ and $a = 10$, then use these kernels in our Dynamic Gamma Knife Radiosurgery Treatment Planning System [38]. Our goal is to let the tumor receive a 2100 cGy dose. Figure 24 shows the DVH comparison. Figure 25 and Figure 26 show the comparisons between dose profiles and isodose distributions. Observe that as ERFC sharpness parameter increases, the target will receive a higher dose and critical structures will receive a lower dose, which means the treatment plan is better. Through the profile comparisons in Figure 25, we notice that DPP plan with $a = 10$ has a lower dose at low dose region than DPP plan with $a = 1$, which means the critical structure will receive a lower dose as the ERFC parameter increases.
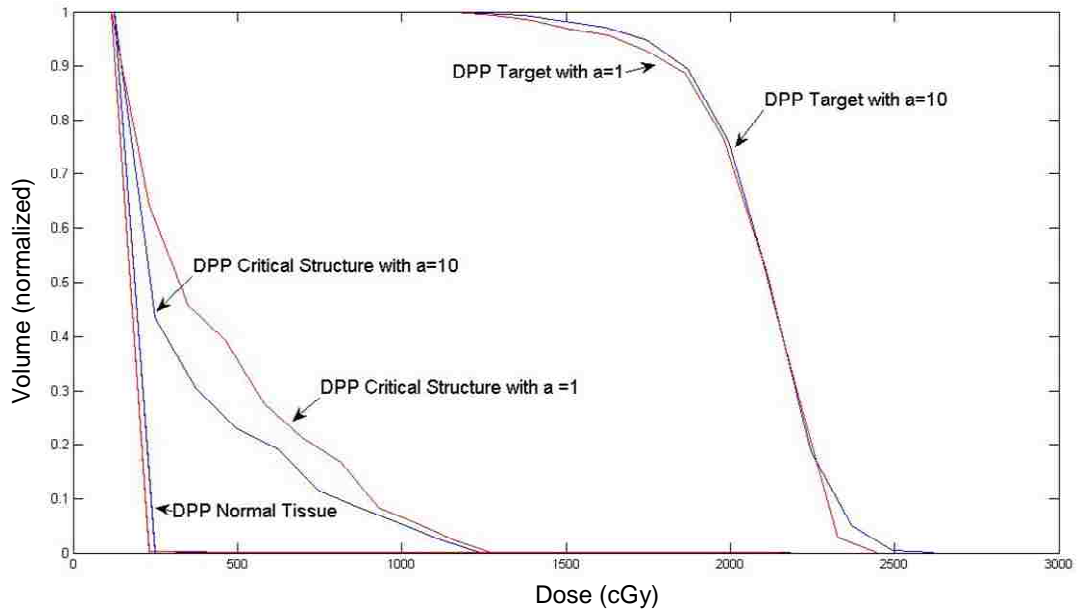
Figure 24 DVH comparison of DPP with $a=1$ and $a=10$ using the C shaped tumor example
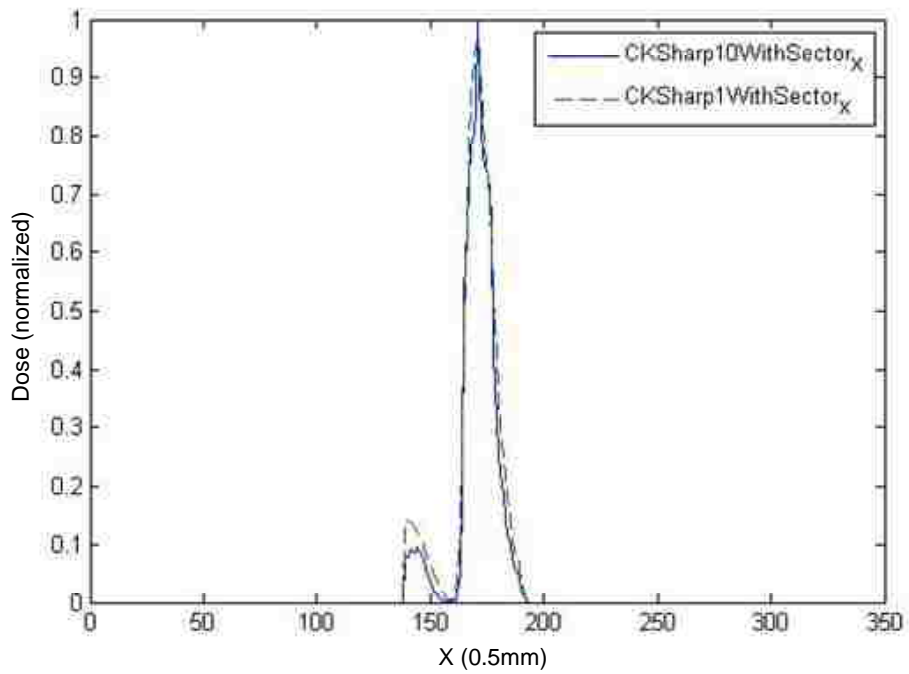
(a)
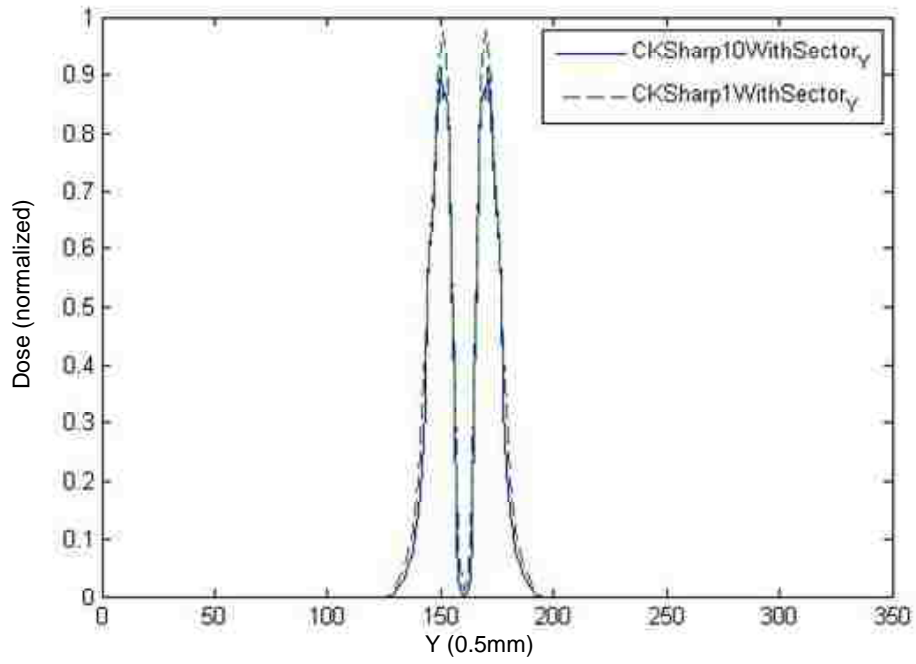
(b)
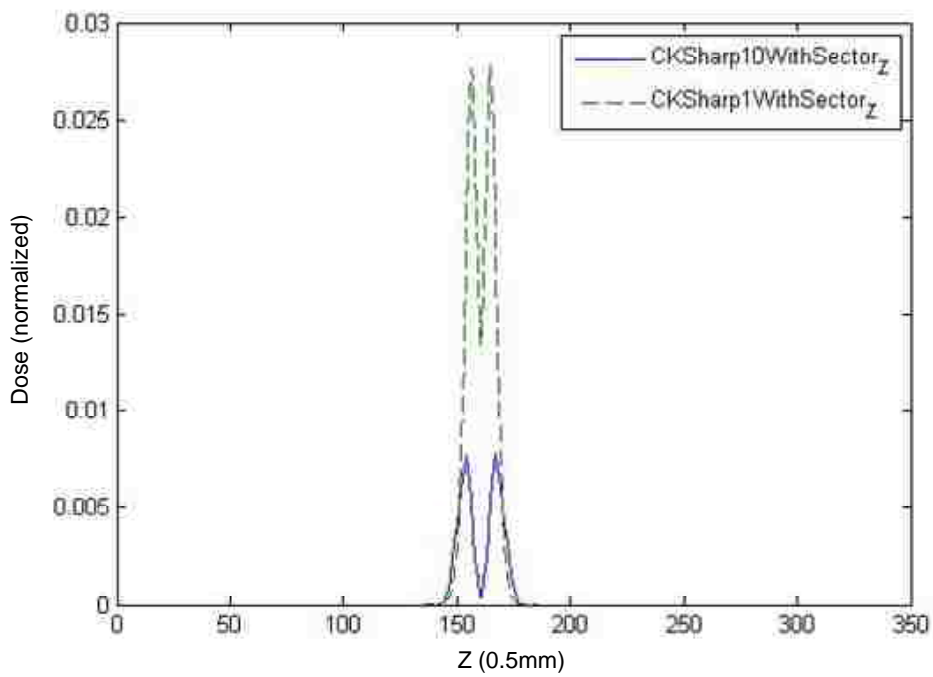
(c)

Figure 25 Dose profile comparisons between DPP plan with $a = 1$ and $a = 10$. (a) Dose profiles along the X direction. (b) Dose profiles along the Y direction. (c) Dose profiles along the Z direction.

(a)

(b)

51
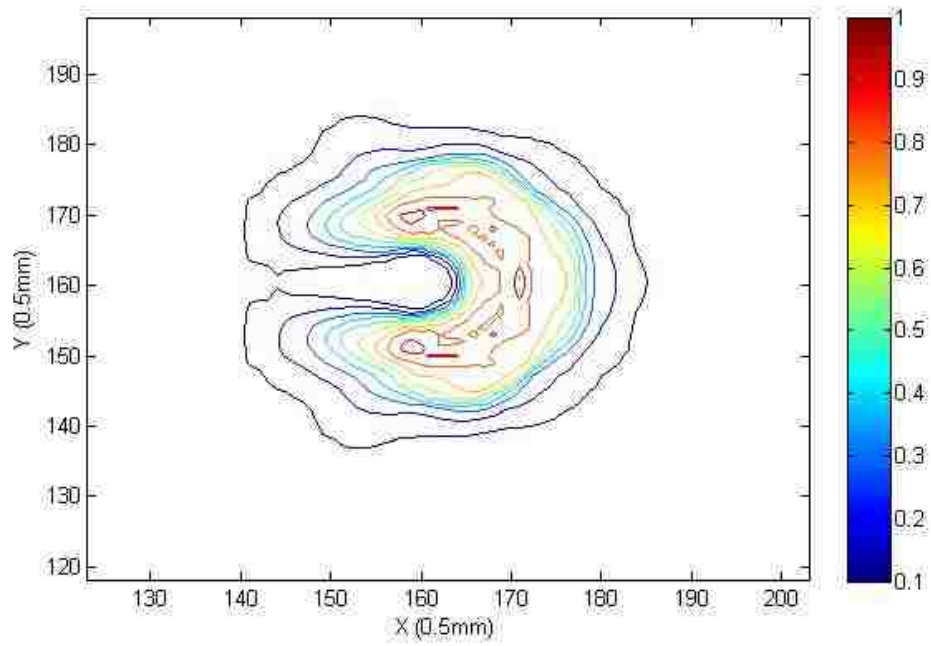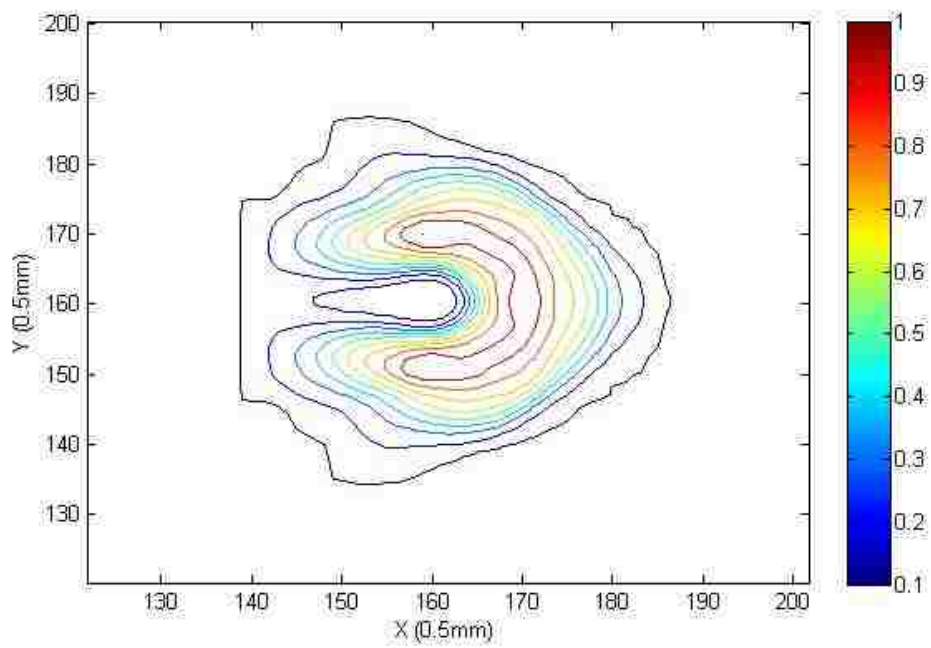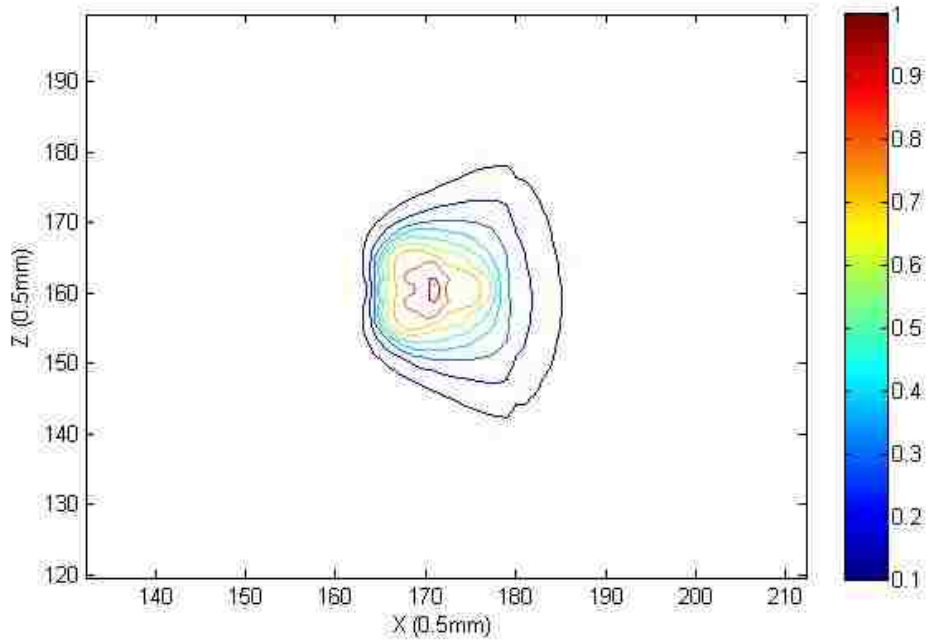
(c)
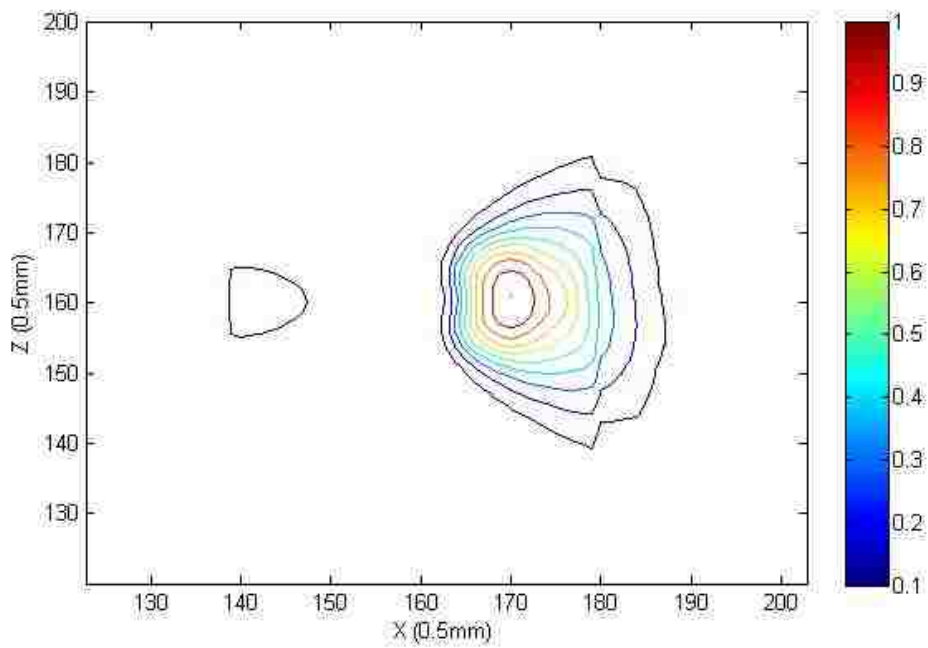
(d)
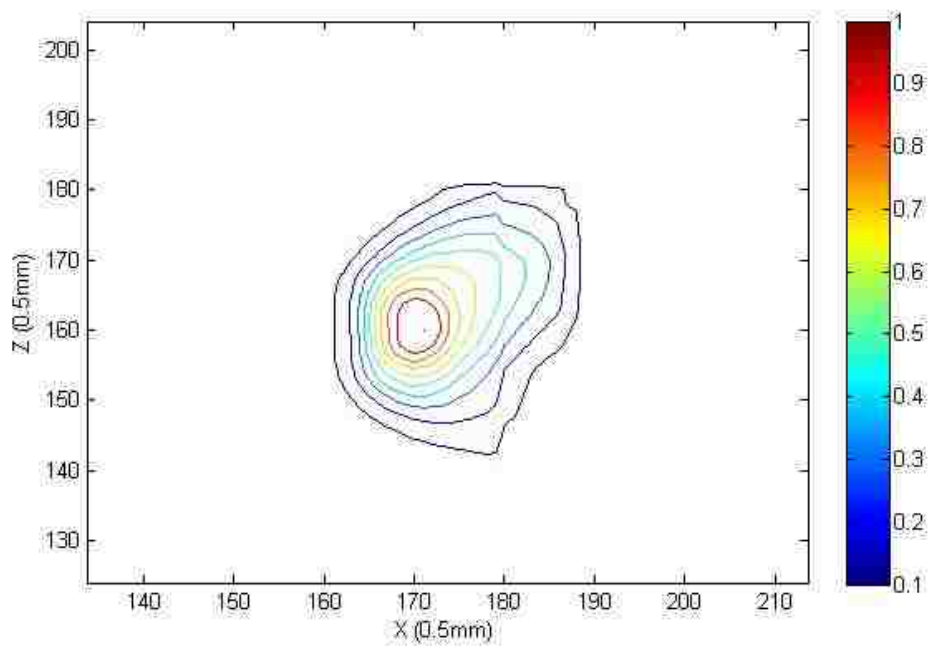
Figure 26 Isodose comparisons between DPP plan with $a = 1$ and $a = 10$. (a) Isodose

distributions of the DPP plan with $a = 10$ in the XY plane. (b) Isodose distributions of

the DPP plan with $a = 1$ in the XY plane. (c) Isodose distributions of the DPP plan with

$a = 10$ in the XZ plane. (d) Isodose distributions of the DPP plan with $a = 1$ in the XZ plane. The plot shown contains isodose lines from 10% to 100% with 10% steps.

4.3 Key Obstacles and Solutions of DPP Implementation

CyberKnife robotic radiosurgery has the potential to implement Dynamic Photon Painting. The computational challenge of optimizing thousands of beams can be solved using cloud computing. Furthermore, various versions of NNLS (Non-Negative Least Square) solvers were implemented to reduce the computational time.

CHAPTER 5 Conclusion and future work

We investigated the possibility of using Dynamic Photon Painting (DPP) for radiation therapy and radiosurgery, and have demonstrated that the DPP approach has the potential to rival proton therapy and Gamma Knife radiosurgeries. The key obstacle of the implementation of Dynamic Photon Painting is computation time, which can be solved by using a multithread method. Various versions of Non-Negative Least Square solvers were implemented to cut down the computational time of the optimization. A prototype of Dynamic Photon Painting treatment planning system is under development.

Reference

[1] Eben Alexander III, Thomas M. Moriarty, Roger B. Davis, Patrick Y. Wen, Howard A. Fine, Peter M. Black, Hanne M. Kooy, Jay S. Loeffler. Stereotactic Radiosurgery for the Definitive, Noninvasive Treatment of Brain Metastases. *Journal of the National Cancer Institute*, 87(1): 34-40, 1995.

[2] Peterson AM, Meltzer CC, Evanson EJ, Flickinger JC, Kondziolka D, MR imaging response of brain metastases after gamma knife stereotactic radiosurgery, *Radiology* 211(3): 807-14, 1999

[3] F. M. L. Amirouche, Tongyi Jia, and Sitki K. Ider. A Recursive Householder Transformation for Complex Dynamical Systems With Constraints. *Journal of Applied Mechanics*, Vol. 55, 1988

[4] Osvaldo Betti, Claudio Munari, Roberto Rosler. Stereotactic Radiosurgery with the Linear Accelerator: Treatment of Arteriovenous Malformations. *Neurosurgery*, Vol. 24, 1989

[5] Smit BM. Prospects for proton therapy in carcinoma of the cervix. *International Journal of Radiation Oncology Biology Physics* 22(2):349-53, 1992

[6] Peter Businger and Gene H. Golub. Linear least squares solutions by householder transformations. *Numerische Mathematik*, p269-276, 2005

[7] Marcello L. R. de Campos, Stefan Werner and José Antonio Apolinário. Constrained Adaptation Algorithms Employing Householder Transformation. *IEEE Transactions on Signal Processing*, Vol. 50, 2002

[8] Christine E. Canman, Dae-Sik Lim, Karlene A. Cimprich, Yoichi Taya, Katsuyuki Tamai, Kazuyasu Sakaguchi, Ettore Appella, Michael B. Kastan, Janet D. Siliciano.

Activation of the ATM Kinase by Ionizing Radiation and Phosphorylation of p53. *Science*, Vol. 281, pp. 1677-1679, 1998

[9] J. Chun, T. Kailath, and H. Lev-Ari. Fast Parallel Algorithms for QR and Triangular Factorization. *SIAM Journal on Scientific and Statistical Computing*, Vol. 8, pp. 899-913, 1987

[10] D. Cochrane and G. H. Orcutt. Application of Least Squares Regression to Relationships Containing Auto- Correlated Error Terms. *Journal of the American Statistical Association*, Vol. 44, pp. 32-61, 1949

[11] Federico Colombo, Antonio Benedetti, Franco Pozza, Renzo Carlo Avanzo, Cristina Marchetti, Giorgio Chierego, Agostino Zanardo. External Stereotactic Irradiation by Linear Accelerator. *Neurosurgery*, Vol. 16, 1985

[12] Shiau CY, Sneed PK, Shu HK, Lamborn KR, McDermott MW, Chang S, Nowak P, Petti PL, Smith V, Verhey LJ, Ho M, Park E, Wara WM, Gutin PH, Larson DA, Radiosurgery for brain metastases: relationship of dose and pattern of enhancement to local control. *International Journal of Radiation Oncology Biology Physics* 37(2): 375-383, 1997

[13] Kondziolka D, Flickinger JC, Bissonette DJ, Bozik M, Lunsford LD, Survival benefit of stereotactic radiosurgery for patients with malignant glial neoplasms, *Neurosurgery* 41(4):776-83, 1997

[14] Larson DA, Gutin PH, McDermott M, Lamborn K, Sneed PK, Wara WM, Flickinger JC, Kondziolka D, Lunsford LD, Hudgins WR, Friehs GM, Haselsberger K, Leber K, Pendl G, Chung SS, Coffey RJ, Dinapoli R, Shaw EG, Vermeulen S, Young RF, hirota M, Inoue HK, Ohy C, Shibazaki T, Gamma knife for glioma: selection factors and survival,

International Journal of Radiation Oncology Biology Physics 36(5): 1045-1053, 1996

[15] Jeffrey W. Degen, Gregory J. Gagnon, Jean-Marc Voyadzis, Donald A. McRae, Michael Lunsden, Sonja Dieterich, Inge Molzahn, and Fraser C. Henderson. CyberKnife stereotactic radiosurgical treatment of spinal tumors for pain control and quality of life. *Journal of Neurosurgery* 2(5):540-9, 2005

[16] Yoshino E, Ohmori Y, et al., Irradiation effects on the metabolism of metastatic brain tumors: analysis by positron emission tomography and 1H-magnetic resonance spectroscopy, *Stereotactic and Functional Neurosurgery*, 1:240-259, 1996

[17] E. Elmroth and F. G. Gustavson. Applying recursion to serial and parallel QR factorization leads to better performance. *IBM Journal of Research and Development*, Vol. 44, 2000

[18] William A. Friedman, Frank J. Bova, and William M. Mendenhall. Linear accelerator radiosurgery for arteriovenous malformations: the relationship of size to outcome. *Neurosurgery*, Vol. 82, 1995

[19] Philip E. Gill and Walter Murray. Algorithms for the Solution of the Nonlinear Least-Squares Problem. *SIAM Journal on Numerical Analysis*, Vol. 15, pp. 977-992, 1978

[20] Thomas E. Goffman, Eli Glatstein. Intensity-Modulated Radiation Therapy. *Radiation Research*, Vol. 158, pp. 115-117, 2002

[21] Gene H. Golub and Charles F. Van Loan. An Analysis Of The Total Least Squares Problem. *SIAM Journal on Numerical Analysis*, Vol. 17, 1980

[22] Monique Guignard. Generalized Kuhn–Tucker Conditions for Mathematical Programming Problems in a Banach Space. *SIAM Journal on Control and Optimization*,

Vol. 7, pp. 232-241, 1969

[23] Brian C. Gunter and Robert A. Van De Geijn. Parallel out-of-core computation and updating of the QR factorization. *ACM Transactions on Mathematical Software (TOMS)*, Vol. 31, 2005

[24] D.A. Jaffray, J.J. Battista, A. Fenster and P. Munro. X-ray sources of medical linear accelerators: Focal and extra-focal radiation. *Medical Physics*, Vol. 20, pp. 1417-1427, 1993

[25] Ganz JC, Gamma knife radiosurgery. *Springer-Verlag*, Australia, 1997

[26] Flickinger JC, Kondziolka D, Lunsford LD, Coffey RJ, Goodman ML, Shaw EG, Hudgins WR, Weiner R, Harsh GR 4th, Sneed PK, et al, A multi-institutional experience with stereotactic radiosurgery for solitary brain metastasis. *International Journal of Radiation Oncology Biology Physics* 28(4): 797-802, 1994

[27] Flickinger JC, Lunsford LD, Wu A et al., Treatment planning for gamma knife radiosurgery with multiple isocenters, *International Journal of Radiation Oncology Biology Physics* 18 (6): 1495-501, 1990

[28] Adler JR, Chang SD, Murphy MJ, Doty J, Geis P and Hancock SL. The CyberKnife: a frameless robotic system for radiosurgery. *Stereotactic and Functional Neurosurgery* 69(1-4 Pt 2):124-8, 1997

[29] Welsh JS, Patel RR, Ritter MA, Harari PM, Mackie TR, Mehta MP. Helical tomotherapy: an innovative technology and approach to radiation therapy. *Technology in Cancer Research and Treatment*, 1(4):311-6, 2002

[30] Faiz M. Khan. The Physics of Radiation Therapy. *Medical Physics*, Vol. 37, pp. 1374-1375, 2010

[31]John S. Kuo, Cheng Yu, Zbigniew Petrovich and Michael L.J. Apuzzo. The CyberKnife Stereotactic Radiosurgery System: Description, Installation, and an Initial Evaluation of Use and Functionality. *Neurosurgery*, Vol. 53, pp 1235-1239, 2003

[32]Ma L, Chin L, DiBiase S, Gullapalli R, Kennedy A, and Marc Simard J. Concomitant boost of stratified target volume with gamma knife radiosurgery: a treatment planning study. *American Journal of Clinical Oncology*, 26(4) 100-105e, 2003

[33]Charles L. Lawson and Richard J. Hanson. Solving Least Squares Problems. *Prentice-Hall, INC*

[34]L Leksell. Stereotactic radiosurgery. *Journal of Neurology, Neurosurgery & Psychiatry*, 46:797-803, 1983

[35]Wald LL, Nelson SJ, Day MR, Noworolski SE, Henry RG, Huhn SL, Chang S, Prados MD, Sneed PK, Larson DA, Wara WM, McDermott M, Dillon WP, Gutin PH, Vigneron DB, Serial proton magnetic resonance spectroscopy imaging of glioblastoma multiforme after brachytherapy, *Journal of Neurosurgery* 87(4): 525-534, 1997

[36]Shuang Luan, Nathan Swanson, Zhe Chen, Lijun Ma. A Prototype Planning System for Dynamic Gamma Knife Radiosurgery. *The American Association of Physics in Medicine*, 2009

[37]Shuang Luan, Nathan Swanson, Lijun Ma, and Li K. Dynamic Gamma Knife Radiosurgery. *The 8th Bi-Annual Congress of International Society of Stereotactic Radiosurgery*, 2007

[38]Shuang Luan, Nathan Swanson, Zhe Chen, Lijun Ma. Dynamic Gamma Knife Radiosurgery. *Physics in Medicine and Biology* 54 1579-1591, 2009

[39] Mikuláš Luptáčik. Kuhn–Tucker Conditions. *Mathematical Optimization and Economic Analysis*, Vol. 36, 2009

[40] T. Rockwell Mackie, John Balog, Ken Ruchala, Dave Shepard, Stacy Aldridge, Ed Fitchard, Paul Reckwerdt, Gustavo Olivera, Todd McNutt and Minesh Mehta. Tomotherapy. *Seminars in Radiation Oncology*, Vol. 9, Pages 108-117, 1999

[41] T. Rock Mackie, Timothy Holmes, Stuart Swerdloff, Paul Reckwerdt, Joseph O. Deasy, James Yang, Bhudatt Paliwal and Timothy Kinsella. Tomotherapy: A new concept for the delivery of dynamic conformal radiotherapy. *Medical Physics*, Vol. 20, pp. 1709-1719, 1993

[42] Helena J. Mauceri, Nader N. Hanna, Michael A. Beckett, David H. Gorski, Mary-Jane Staba, Kerri Anne Stellato, Kevin Bigelow, Ruth Heimann, Stephen Gately, Mohanraj Dhanabal, Gerald A. Soff, Vikas P. Sukhatme, Donald W. Kufe and Ralph R. Weichselbaum. Combined effects of angiostatin and ionizing radiation in antitumour therapy. *Nature* 394, 287-291, 1998

[43] W. Morven. Least Squares Computations by Givens Transformations Without Square Roots. *IMA Journal of Applied Mathematics* 12(3):329-336, 1973

[44] Mehta MP, Rozental JM, Levin AB, Mackie TR, Kubsad SS, Gehring MA, Kinsella TJ. Defining the role of radiosurgery in the management of brain metastases. *International Journal of Radiation Oncology Biology Physics*, 24(4):619-25, 1992

[45] Karl Otto. Volumetric modulated arc therapy: IMRT in a single gantry arc. *Medical Physics*, Vol. 35, pp. 310-317, 2008

[46] Christopher C. Paige and Michael A. Saunders. LSQR: An Algorithm for Sparse

Linear Equations and Sparse Least Squares. *ACM Transactions on Mathematical Software (TOMS)*, Vol. 8, 1982

[47] Christoph von Praun and Thomas R. Gross. Static conflict analysis for multi-threaded object-oriented programs. *ACM Sigplan Notices*. Vol. 38, 2003

[48] Young RF, The role of the gamma knife in the treatment of malignant primary and metastatic brain tumors, *CA Cancer J Clin* 48(3): 177-88, 1998

[49] Stephen M. Robinson. Perturbed Kuhn-Tucker points and rates of convergence for a class of nonlinear-programming algorithms. *Mathematical Programming*, Vol. 7, 1974

[50] R. T. Rockafellar and R. J. -B. Wets. Stochastic convex programming: Kuhn-Tucker conditions. *Journal of Mathematical Economics*, Vol. 2, Pages 349-370, 1975

[51] DiBiase S, Chin L, and Ma L. "The influence of Gamma Knife radiosurgery on the quality of life in patients with brain metastases", *American Journal of Clinical Oncology*, 25(2): 131-134, 2002

[52] Daniela Schulz-Ertner and Hirohiko Tsujii. Particle Radiation Therapy Using Proton and Heavier Ion Beams. *Journal of Clinical Oncology*, Vol. 25, pp. 953-964, 2007

[53] Seung SK, Sneed PK, McDermott MW, Shu HK, Leong SP, Chang S, Petti PL, Smith V, Verhey LJ, Wara WM, Phillips TL, Larson DA, Gamma knife radiosurgery for malignant melanoma brain metastases. *Cancer Journal From Scientific American* 4(2): 103-9, 1998

[54] Wasserman TH, Larson D, Shaw EG, Stereotactic Radiosurgery, Journal of Clinical Oncology 17: 615-621, 1999

[55] Nai-Kuan Tsao. A Note on Implementing the Householder Transformation. *SIAM Journal on Numerical Analysis*, Vol. 12, pp. 53-58, 1975

[56] Dean M. Tullsen, Susan J. Eggers and Henry M. Levy. Simultaneous multithreading: maximizing on-chip parallelism. *International Symposium on Computer Architecture*, Pages: 392 – 403, 1995

[57] Lutz W, Winston KR and Maleki N. A system for stereotactic radiosurgery with a linear accelerator. *International Journal of Radiation Oncology Biology Physics* 14(2):373-81, 1988

[58] Chao Wang, Shuang Luan, Grace Tang, Danny Z Chen, Matt A Earl and Cedric X Yu. Arc-modulated radiation therapy (AMRT): a single-arc form of intensity-modulated arc therapy. *Physics in Medicine and Biology* 53 6291, 2008

[59] Ken Winston, Wendell Lutz. Linear Accelerator as a Neurosurgical Tool for Stereotactic Radiosurgery. *Neurosurgery*, Vol. 22, 1988

[60] Cedric X Yu. Intensity-modulated arc therapy with dynamic multileaf collimation: an alternative to tomotherapy. *Physics in Medicine and Biology*, 1995

[61] Intensity Modulated Radiation Therapy Collaborative Working Group. Intensity-modulated radiotherapy: current status and issues of interest. *International Journal of Radiation Oncology Biology Physics*, Vol. 51, Pages 880-914, 2001

[62] Accuray. http://www.accuray.com/

[63] Elekta Gamma Knife Radiosurgery. http://www.elekta.com/

[64] Fluka. http://www.fluka.org/fluka.php?id=man_onl&sub=0

[65] GCC manual. http://gcc.gnu.org/onlinedocs/

[66] Wolfram Math World. http://mathworld.wolfram.com/Erfc.html